# Effects of TiO$_2$ Nanoparticles on the Overall Performance and Corrosion Protection Ability of Neat Epoxy and PDMS Modified Epoxy Coating Systems

*Ammar Shafaamri[1]\*, Chiam H. Cheng[1], Iling A. Wonnie Ma[1], Shahid B. Baig[1], Ramesh Kasi[1]\*, Ramesh Subramaniam[1] and Vengadaesvaran Balakrishnan[2]*

[1] Department of Physics, Center for Ionics University of Malaya, University of Malaya, Kuala Lumpur, Malaysia, [2] UM Power Energy Dedicated Advanced Centre (UMPEDAC), University of Malaya, Kuala Lumpur, Malaysia

Epoxy-TiO$_2$ nanocomposite coatings were prepared by the utilization of the solution intercalation method with the presence of the sonication process and the influence of embedding different loading ratios of TiO$_2$ nanoparticles within neat epoxy resin was investigated. To further improve the corrosion protection performance and to fulfill the hydrophobicity of the developed coated surfaces, the epoxy polymeric resin was modified with polydimethylsiloxane (PDMS) and different loading ratio of TiO$_2$ nanoparticles was intoduced to the modified polymeric matrix to fabricate PDMS modified epoxy nanocoposite coating sytems. All developed coating systems were characterized by means of Fourier transform infrared (FTIR) spectroscopy and differential scanning calorimetry (DSC) to investigate the chemical structure and the glass transition temperatures (T$_g$) of the developed coating systems, respectively. The morphology, topology, optical properties, and the wettability were also examined by field emission scanning electron microscope (FESEM), energy dispersive X-rays analyzer (EDX), atomic force microscopy (AFM), ultraviolet-visible spectroscopy (UV-vis), and contact angle measurement (CA), respectively. Moreover, the electrochemical behavior and the barrier properties of the developed coating films were investigated via electrochemical impedance spectroscopy (EIS). The findings revealed a good curing level with higher T$_g$ values for all developed nanaocompsoite coating systems and confirmed the efficiency of the sonication process in developed well-dispersed TiO$_2$ within the polymeric matrix. Also, the obtained results revealed the ability of certain amount of TiO$_2$ nanoparticles in enhancing the corrosion protection performance of epoxy based coating systems. The compatibility of epoxy resin, PDMS, and TiO$_2$ nanoparticles was also confirmed by achieving the hydrophobicity and obtaining the best corrosion protection performance.

**Keywords: epoxy, polydimethylsiloxane (PDMS), TiO$_2$ nanoparticles, nanocomposite coatings, hydrophobic, electrochemical impedance spectroscopy (EIS)**

# INTRODUCTION

Due to atmospheric interaction with the environment, corrosion can be defined as the degradation of metallic material via electrochemical reaction on its surface, where it can cause damage and destruction of the material. Moreover, it can lead to an economic burden to a country and put risk to human being's health and safety. Preservation to protect metallic material by applying protective coating is the best practice to overcome most of the corrosion issues and consequences across the globe. The polymeric coating is to provide barrier property on material surface and has been an outstanding choice for anticorrosion purpose due to its production accessibility. However, polymer resin has its shortcoming sustainability that it contains free volume, micro-voids, and exhibits hydrophilicity due to their polar group which gives strong affinity toward water molecules (Ammar et al., 2016b; Guo et al., 2018). These drawbacks lead corrosion process through diffusion of corrosive agents such as oxygen, water molecules, and aggressive anions, create deterioration pathways to reach the coating-metal interface. This action is known as penetration which caused localized corrosion on the material surface that responsible for the damage via hydrolytic degradation (Zaarei et al., 2008; Heidarian et al., 2010; Brusciotti et al., 2013; Verma et al., 2019). A huge number of researches have been done to improve the barrier properties of the polymeric coating in the past decades (Dolatzadeh et al., 2011; Heidarian et al., 2011; Shen and Zuo, 2014; Matin et al., 2015; Mohamad Saidi et al., 2018; Zheng et al., 2019). By incorporating nano-sized fillers into the polymer resin, it is aimed that this effort will enhance the anticorrosion and barrier properties of the polymer coating via various mechanisms, such as filling up the pores and reducing the matrix defects, bowing, bridging and deflecting the cracks (Ammar et al., 2016c). Also, the inorganic nano-sized filler tends to function as a connecting bridge linking between the matrix molecules, thus reducing the total free volume and promotes cross-linking (Shi et al., 2009; Heidarian et al., 2010; Atta et al., 2019). These mechanisms, in turn, delay the penetration activity which slows down the diffusion of corrosive agents in the coating layer from reaching to the coating-metal interface, thus decreasing the corrosion rate on the material surface. One of the utilizable nano-size filler is Titanium dioxide ($TiO_2$) nanoparticles which have been used extensively due to its ability to provide a photocatalytic effect (Liqiang et al., 2003). This means that it is capable to release a huge number of electrons when exposed to ultraviolet light radiation. These electrons then initiate the photo-induced redox reaction on the corrosion causing agents that are adsorbed on the coating surface, further curbing corrosion reaction. Worth to note that ultraviolet light can release radicals which will be able to break the molecular structure of neat polymeric coating layer. Nevertheless, this mechanism provides it an antimicrobial property to kill bacteria that are present on the coating surface, which may also act as corrosion causing agent (Fu et al., 2005; Evans and Sheel, 2007). By that, $TiO_2$ nanoparticles are extensively used due to their anti-fouling, self-cleaning and also odor-inhibition properties resulting from the photocatalytic effect they exhibit.

However, due to the high porosity and hydrophilicity properties possessed by the polymer resin, it drags down the performance of anticorrosion properties by the developed coating system as water molecule is one of the most easily be-in-contact corrosions causing agent. Silicones are categorized as a type of high-valued polymers due to its capability to affect the efficacy of various applications in the industrial field (Eduok et al., 2017; Liao et al., 2018). It gives a significant impact on the industrial applicated due to its molecular structure that may exist in assorted forms (Pouget et al., 2009). Silicone polymers are widely used as polydimethylsiloxane (PDMS) which is an inorganic polymer and has the properties of being hydrophobic contributed by its non-polar -$CH_3$ group that gives the coating low surface energy (Ammar et al., 2017). Massive research works have been conducted in the past few years (Sung and Lin, 1997; Velan and Bilal, 2000; Ahmad et al., 2005) to determine the optimum mixing ratio between epoxy resin and PDMS. It has been agreed that the mixing ratio of 90:10 w/w gives the most optimum performance, especially on the research outcome performed by Ananda Kumar together with his research team (Kumar and Narayanan, 2002; Kumar et al., 2002, 2006; Duraibabu et al., 2014).

In this study, a simple preparation method was developed to prepare the epoxy-$TiO_2$ nanocomposite coating systems. As a result, a homogeneous solution with different $TiO_2$ loading ratios incorporated in epoxy resin was successfully prepared. Then, additional systems were amended with PDMS as modifier into epoxy-$TiO_2$ nanocomposite to develop epoxy-PDMS hybrid polymeric coating systems. The aims for both developed coating systems are to study the effect of low concentration of $TiO_2$ in two different polymeric based, epoxy and epoxy-PDMS matrices. The structure, thermal, and optical properties of all developed coating systems were investigated by FTIR, DSC, and UV-Vis, respectively. Moreover, FESEM, EDX, and AFM were employed to reveal the morphologies of the developed systems. The wettability of the resultant systems was determined by using contact angle method. As for, the barrier properties of the developed coating systems and the corrosion protection performance were investigated via EIS after exposing the cold rolled mild steel coated substrates to 3.5% NaCl solution up to 30 days.

# EXPERIMENTAL

## Materials

Epoxy resin (EPIKOTE 828) produced from a polycondensation reaction between bisphenol A and epichlorohydrin with an equivalent weight of 184–190 g/eq and viscosity of 12,000–14,000 cP at room temperature was purchased from Asachem (Malaysia) and used as the base resin. Modifier used was hydroxyl-terminated polydimethylsiloxane (HT-PDMS) with a viscosity of 750 cSt and a density of 0.97 g/ml at room temperature was supplied by Sigma-Aldrich (Malaysia) and used as the modifier for the epoxy resin. In order to develop the hybrid epoxy-PDMS polymeric matrix, 3-aminopropyltriethoxysilane (KBE-903) purchased from Shin-Etsu Chemical Co. Ltd (Japan) was used as the coupling agent. The development of all

nanocomposite coating systems was carried out via the utilization of titanium (IV) oxide nanoparticles of anatase crystalline structure with diameter < 25 nm and density of 3.9 g/mL at room temperature which was supplied by Sigma-Aldrich (Malaysia). Cycloaliphatic amine with an amine value of 260–285 mg KOH/g and an equivalent weight of 113 g/eq and acted as the curing agent and purchased from Hexion (Malaysia). All listed chemicals were used as received from the supplier without any further modification or purification.

## Substrates Preparation and Coating Application

Cold rolled mild steel substrates with dimensions of 5 × 7.5 × 0.1 cm were employed as the tested substrate to be coated. The steel panels were first degreased and cleaned using acetone then the pretreated specimens were subjected to sandblasting process according to ASTM D609 standard to achieve Sa 2½ surface profile followed by wiping the resulted surfaces with acetone once again to clean off the dust and any other impurities deposited from the sandblasting process. The brushing method was used to developed all coating films which were kept to dry for 7 days at room temperature. The dry film thickness was selected to be in the range of 75 ± 5 μm and was tested via using Elcometer 456 thickness gauge for three replicate coated panels. The coated steel substrates were used to perform FESEM and EIS tests. However, free films were cast onto Teflon plates in order to obtain FTIR testing samples. Transparent glass plates with a size of 2.54 × 7.62 × 0.12 cm were also prepared and subjected to one side coating in order to perform AFM, contact angle measurements and ultraviolet-visible spectroscopy tests.

## Preparation of Coating Systems

Neat epoxy coating system designated as (E) and cured with cycloaliphatic amine at mixing ratio (10:6) was developed and used as the reference system. The epoxy and curing agent blend was subjected to continuous stirring for 15 min at 750 rpm prior to the coating application. Different loading ratio of TiO$_2$ nanoparticles specifically, 0.1, 0.2, and 0.3 wt. % were utilized in order to prepare three different systems of epoxy-based nanocomposite coating systems named as ET1, ET2, and ET3, respectively. For this end, the different loading ratios of TiO$_2$ nanoparticles were first introduced to the calculated amount of the cycloaliphatic amine curing agent with the assistance of sonication process for 30 min. Then the epoxy resin was added and the resulting blend was subjected to sonication process for 10 min followed by constant stirring for 15 min at 750 rpm. Better dispersion state of the TiO$_2$ nanoparticles was expected to be achieved by introducing the nanofillers to the curing agent first followed by mixing the resulting blend with the epoxy base resin. This idea was supported by the 2017 work of Pourhashem et al., that reported the efficiency of this method in developing better dispersion of graphene oxide nanosheets within epoxy resin with the presence of polyamide curing agent which is characterized with lower viscosity comparing to epoxy resin (Pourhashem et al., 2017). To further improve the corrosion protection performance and to fulfill the hydrophobicity of the developed coated surfaces, the epoxy resin was modified with PDMS at (9:1)

mixing ratio with the presence of 3-aminopropyltriethoxysilane as a coupling agent. Prior to the addition of the curing agent, epoxy resin, PDMS, and a stoichiometric equivalent of 3-aminopropyltriethoxysilane were mixed using a glass rod until the mixture appeared to be homogeneous. Then the resulting blend together with the calculated amount of cycloaliphatic amine curing agent was magnetically stirred for 15 min at 750 rpm and then applied on both sides of cold rolled mild steel substrate as EP coating system. Then, the modified epoxy-PDMS polymeric blend was used as the host matrix for different loading ratios of TiO$_2$ nanoparticles specifically, 0.1, 0.2, and 0.3 wt. % in order to fabricate EPT1, EPT2, and EPT3 nanocomposite coating systems, respectively. The TiO$_2$ nanoparticles and cycloaliphatic amine blends were subjected to 30 min of sonication process prior to the addition of epoxy resin, PDMS and 3-aminopropyltriethoxysilane. The resulting mixtures were then subjected to sonication process for 10 min and mechanical stirring for 15 min at 750 rpm.

## Characterization
### Fourier Transform Infrared Spectroscopy (FTIR)
Fourier transform infrared spectroscopy (FTIR) was utilized for structural analysis. ATR-Nicolet iS10 Spectrometer from Thermo Fisher Scientific (USA) was used to obtain FTIR transmission spectra with a 32-scan data accumulation between the wavenumber of 400–4,000 cm$^{-1}$ at a resolution of 4.0 cm$^{-1}$ was acquired for all recorded spectra.

### Differential Scanning Calorimetry (DSC)
The glass transition temperatures (T$_g$) of all developed coating systems was investigated by differential scanning calorimetry (DSC) using Perkin Elmer DSC800 (USA). The temperature range was varied from 25°C to 300°C with heat rate at 20°C/min under nitrogen condition with flow rate with 20 ml/min.

### Field Emission Scanning Electron Microscope (FESEM)
The surface morphology and the dispersion state of the nano TiO$_2$ nanoparticles within the polymeric matrix was investigated by using field emission scanning electron microscopy (FESEM) FEI Quanta 450 FEG equipped with an energy dispersive X-rays analyzer (EDX) for elements mapping. It is worth to be mentioned that the coated steel panels were subjected to the application of a thin layer of a platinum coating before carried out the tests in order to minimize the charging effects.

### Atomic Force Microscopy
A Bruker Multimode 8 AFM was employed for topography imaging and to measure the surface roughness of all coating systems. The measurement of the effect of TiO$_2$ nanoparticle in the coating system was conducted in the contact mode equipped with Scan Asyst-Air (Bruker) SPM tip (0.4 N/m spring constant). The 3D 5 μm$^2$ scanned areas were sampled at 769 equidistant points at a low scan rate of 1 Hz.

### Ultraviolet-Visible (UV-Vis) Spectroscopy
To determine the photocatalytic effects of the incorporated TiO$_2$ nanoparticles, ultraviolet-visible (UV-vis) spectroscopy was used

with UV-3101PC (Shimadzu, Kyoto, Japan) UV-vis spectrometer in transmission mode at a wavelength range of 200–800 nm on medium-speed scanning. The UV-vis spectrometer was set in absorbance mode at the wavelength between 200 and 800 nm range and medium scanning speed. Measurements were carried out on a set of three different replicate coated glass plates.

## Contact Angle (CA) Measurement

Contact Angle (CA) measurements were conducted in order to evaluate the wettability of coated surfaced and distinguish the effects of the embedded $TiO_2$ nanoparticles and modification epoxy resin with PDMS on the surface hydrophobicity state. By using Optical Contact Angle 15EC (Germany) instrument, the static contact angles were obtained by placing 5 drops of 9 μL distilled water at five different points on each coating samples with the use of a needle that located close enough to the coated surface to render the kinetic energy of the droplets negligible. Measurements were repeated for three times on three different coated samples. The results in the form of images were captured instantly and the average of five measurements was reported with <1° measurement error.

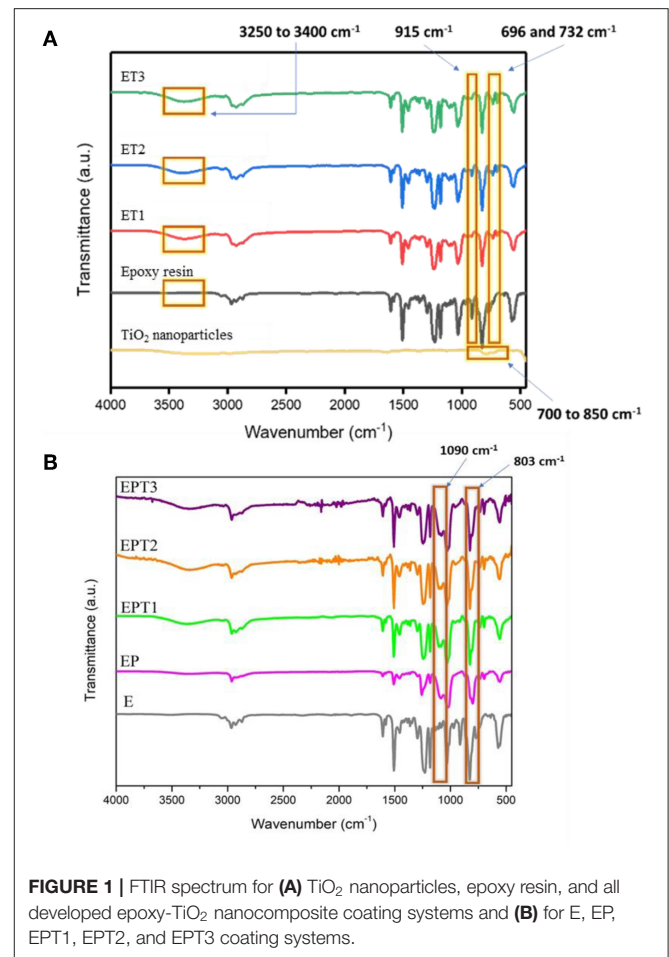## Electrochemical Impedance Spectroscopy (EIS)

In order to evaluate the anticorrosion performance and the barrier properties for all the developed coating systems, electrochemical impedance spectroscopy (EIS) was employed. The EIS was brought in action using a classical three electrode system consisting of 3 $cm^2$ area of the coated sample exposed to 3.5% NaCl distilled water solution as working electrode, a saturated calomel electrode SCE as a reference electrode and pyrolytic graphite electrode functioning as a counter electrode. All the components and connections were placed inside a Faraday cage to minimize external noise during measurement. Gamry PCI4 G300 potentiostat with 100 kHz−10 mHz frequency range at open circuit potential with a sinusoidal AC perturbation of 10 mV root mean square (rms) potential perturbation was used to perform the tests was utilized to complete the test. All the data obtained from EIS were analyzed by Gamry Echem Analyst of Version 6.03. EIS measurements were found to be reproducible after repeating the tests for three different coated substrates.

## RESULTS AND DISCUSSION

### Fourier Transform Infrared Spectroscopy (FTIR)

**Figure 1A** shows the FTIR spectra for $TiO_2$ nanoparticles, epoxy resin, and epoxy-$TiO_2$ nanocomposite coating systems. Most of the peaks in the coating systems can be traced back to the epoxy resin. Note that the epoxy resin spectrum in **Figure 1A** is the uncured epoxy resin.

The FTIR spectrum of $TiO_2$ nanoparticle with anatase crystalline structure showed a broad peak at 700–850 $cm^{-1}$ and was attributed to Ti-O stretching vibration (Vasei et al., 2014). With the incorporation of $TiO_2$ nanoparticles into epoxy resin (ET1, ET2, and ET3), it can be slightly observed on the overlapping peaks that occurred between 700 and 850 $cm^{-1}$ due to low percentage of $TiO_2$ nanoparticles presence in the epoxy



**FIGURE 1 |** FTIR spectrum for **(A)** $TiO_2$ nanoparticles, epoxy resin, and all developed epoxy-$TiO_2$ nanocomposite coating systems and **(B)** for E, EP, EPT1, EPT2, and EPT3 coating systems.

matrix. Compared with epoxy resin spectrum, the absorption band at 696–732 $cm^{-1}$ varies with the nanocomposites were corresponded to Ti-O-Ti linkages in conjunction with the amine group of curing agent and epoxy matrix. This proves that $TiO_2$ nanoparticles are successfully obtained and incorporated into the organic matrix as the epoxy resin is being cured.

The absorption peak at 915 $cm^{-1}$ of unmodified epoxy resin indicates the C-O deformation in the epoxide group, however, the decreased in the intensity of the peak at 915 $cm^{-1}$ in the spectra of cured nanocomposite systems evincing the opening of the epoxide ring during curing reaction. Many studies have reported the curing reactivity of epoxy resin by using amine curing agents (Ansari et al., 2014; Moura et al., 2018). As reported by Ma et al., the curing state of epoxy resin with diamine curing agent at room temperature could be assigned to the disappearance of the absorption peak at 915 $cm^{-1}$ in the cured neat epoxy (Ma et al., 2017). Also, the emergence of a new peak at 3,250–3,400 $cm^{-1}$ in the cured systems instead of unmodified epoxy resin affirmed the existence of secondary amine, which is due to the stretching of the N-H bond. These peaks further assured the curing agent successfully functioned to cure the coating mixture into a film. This to be said that almost all epoxy resins are converted into

insoluble solid film due to the formation of three-dimensional thermoset networks by curing agent during the curing period (Shi et al., 2009; Ma et al., 2017).

**Figure 1B** depicts the FTIR spectra for unmodified epoxy resin (E), epoxy-PDMS hybrid (EP), and PDMS modified epoxy nanocomposite coating systems which are EPT1, EPT2, and EPT3. Note that 3-Aminopropyltriethoxysilane (3-APS) was used to link between epoxy and PDMS resins, thus, the cross-linking between the two polymers can be observed at some fundamental peaks. With the peaks that originate from the consequences of curing reaction as mentioned earlier still to be seen here, the new emerging peak at 803 and 1,090 $cm^{-1}$ is ascribed to the stretching of Si-O-Si and Si-C bond which is not seen in the unmodified epoxy resin. This affirmed that PDMS was successfully incorporated with epoxy forming the desired hybrid coating systems. The coupling mechanism between epoxy and PDMS can be divided into two stages where the first stage involves the opening of the epoxide ring to react with the amino group of the 3-APS, where the primary amine tends to transform to the tertiary amine. During the second stage, PDMS tends to react with epoxy by the endorsement of the alkoxy group in 3-APS, forming the final modified epoxy-silicone structure. Moreover, the disappearance of the band 915 $cm^{-1}$ of the unmodified epoxy spectrum has attributed the opening of the epoxide ring which revealed the intercalation of the curing agent in the epoxy matrix. A similar observation of cured epoxy-PDMS has also been reported by Ammar et al. (2016b). Also form **Figure 1B**, it can be seen the intensity spectra of EPT1, EPT2, and EPT3 are slightly increased as the amount of $TiO_2$ increased. This to be said that the presence of $TiO_2$ nanoparticle within the hybrid polymer matrices is observable on the overlapping peaks occurred between 700 and 850 $cm^{-1}$ as in ET systems (**Figure 1A**). Dan et al. (2018) have reported the possible reason for weak peak appearance which almost invisible on these peaks could be due to the low content of $TiO_2$ filler in the host domain and possibly can be observed at high loading concentration of $TiO_2$, that is, 10 wt.%.

## Differential Scanning Calorimetry (DSC)

The DSC thermographs of E, EP, and all $TiO_2$ nanocomposite coating systems were illustrate in **Figures S1–S8**. Moreover, the glass transition temperatures ($T_g$) values were tabulated

**TABLE 1** | The glass transition temperatures ($T_g$) values of all developed coating systems.

| System | $T_g$ (°C) |
|---|---|
| E | 127.9 |
| ET1 | 143.9 |
| ET2 | 137.5 |
| ET3 | 135.3 |
| EP | 134.2 |
| EPT1 | 142.3 |
| EPT2 | 136.8 |
| EPT3 | 131.4 |

in **Table 1**. A single glass transition temperature was observed in all reported thermographs which indicate the good curing state of the coating films and the proper crosslinking among the coating components (Radoman et al., 2014; Ammar et al., 2016b). However, the changes in the $T_g$ values could be utilized as an indicator that illustrates the influences of PDMS and $TiO_2$ nanoparticles on the cross-linked structure of the epoxy polymeric matrix. As tabulated in **Table 1**, the incorporation 0.1 wt. % of $TiO_2$ nanoparticles within the epoxy polymeric matrix had the most pronounced effect on the $T_g$ value which increased from 127.9°C for neat epoxy coating system to ~144°C ET1. Similar observations were reported by Radoman et al. (2015), who claimed that the epoxy resin is able to exhibit higher $T_g$ values when it reinforced with $TiO_2$ nanoparticles due to the role of these particles in reducing the segments mobility at the nanoparticles-epoxy interfaces by the presence of physical attractive interactions.

Apart from that, further increasing the concentration of $TiO_2$ nanoparticles within the epoxy host matrix did not result in higher $T_g$ values, contrarily, relatively lower $T_g$ values, comparing to ET1 coating system, were recorded for ET2 and ET3 systems. This reduction in the $T_g$ values could be ascribed to the insufficient dispersion of $TiO_2$ nanoparticles and its tendency to agglomerate and cluster at the high concentrations. This trend of the nanoparticles physically hinders the curing process of the coating system by blocking the formation of the continuous crosslinked network, hence, increasing the free volume and the mobility of the segments (Polizos et al., 2011; Kumar et al., 2016).

On the other hand, modifying the epoxy resin with PDMS has also influence the glass transition temperature of the resultant coating system which recorded an increment in the $T_g$ value at 134.3°C. This was found in good correlation with FTIR results and further confirmed the good crosslinked structure among epoxy and PDMS resin. The effects of the $TiO_2$ nanoparticles on the thermal properties of the PDMS-epoxy polymeric matric were found to be similar to their influences to the neat epoxy polymeric matrix as the coating system with 0.1 wt. % of $TiO_2$ loading ratio, EPT1, demonstrated the highest $T_g$ value. Whereas, higher concentrations of $TiO_2$ nanoparticles reduce the $T_g$ values due to the agglomeration tendency of the nanoparticles.

## Surface Morphology

In order to examine the dispersion state of the embedded $TiO_2$ nanoparticles within the epoxy polymeric matrix, FESEM, and EDX techniques were utilized and the recorded images were illustrated in **Figure 2**. In addition to studying the distribution of the nanoparticles within the surface area, the surface properties, and phase distribution can be evaluated via FESEM. Moreover, the EDX mapping helps on gaining more understanding about the element distribution in the coating film and investigating the dispersion state of $TiO_2$ nanoparticles at the specimen surface. All developed epoxy-based nanocomposite coatings demonstrated surfaces free of microcracks or phase separation which is clear evidence on the effectiveness of the curing process. Moreover, the vital role of the sonication process was observed in all FESEM images that revealed a good dispersion of the nanoparticles. Due to the attraction among the nanoparticles
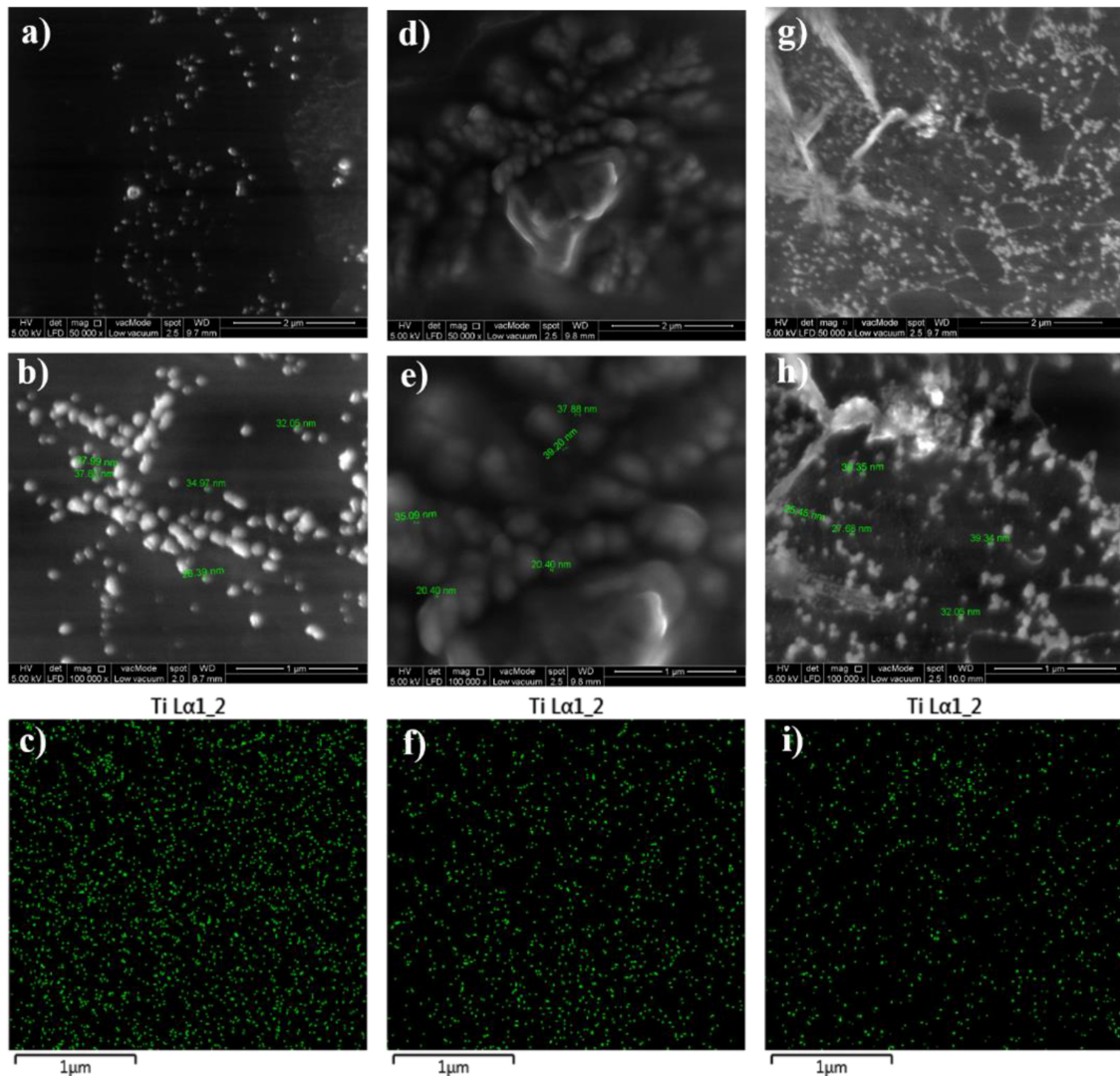
**FIGURE 2 |** FESEM images at x50000 and x100000 magnifications together with EDX mapping images for ET1 **(a–c)**, ET2 **(d–f)**, and ET3 **(g–i)**.

and its tendency to form relatively larger agglomerated particles, the agglomeration increases as the $TiO_2$ nanoparticle loading ratio exceeds 0.1 wt. %. Moreover, the proper dispersion state of $TiO_2$ nanoparticles was further confirmed by EDX mapping results which illustrate the distribution of Ti element on the coated surfaces. In addition, the surface morphology of the $TiO_2$ nanocomposite coatings that developed after modifying the epoxy host matrix with PDMS resin was investigated and the FESEM and EDX images were illustrated in **Figure 3**. Surface free of cracks and phase separation confirms the compatibility of the coating components and the good curing level of the coating films. However, it was noticed that as the loading ratio of the $TiO_2$ nanoparticles increase, larger clusters were observed in the FESEM images especially for EPT3 coating systems. That could be attributed due to the tendency of the nanoparticles to agglomerate at the high loading ratio and to the increase of the particles amount within the unit area. EDX mapping images

were also collected for this set of samples and the results reveled the existence of well-dispersed Ti element within the coating film which is considered as a clear evidence on the appropriate introduction of $TiO_2$ nanoparticles within the hybrid PDMS-epoxy polymeric matrix.

## Atomic Force Microscopy (AFM)

The topological properties of the developed coating systems and the changes in the surface roughness were investigated by means of AFM. **Figure 4** illustrates the 3 D topographical images of neat epoxy and all developed epoxy-$TiO_2$. nanocomposite coating systems. The AFM result of the neat epoxy coating system revealed a root mean square height (Sq) equal to 15.5 nm, whereas, Sq values at 2.5, 3.6, and 10.2 nm were recorded to ET1, ET2, and ET 3 coating systems, respectively. The high surface roughness of the neat epoxy coating system could be attributed to the solvent evaporation during the curing period
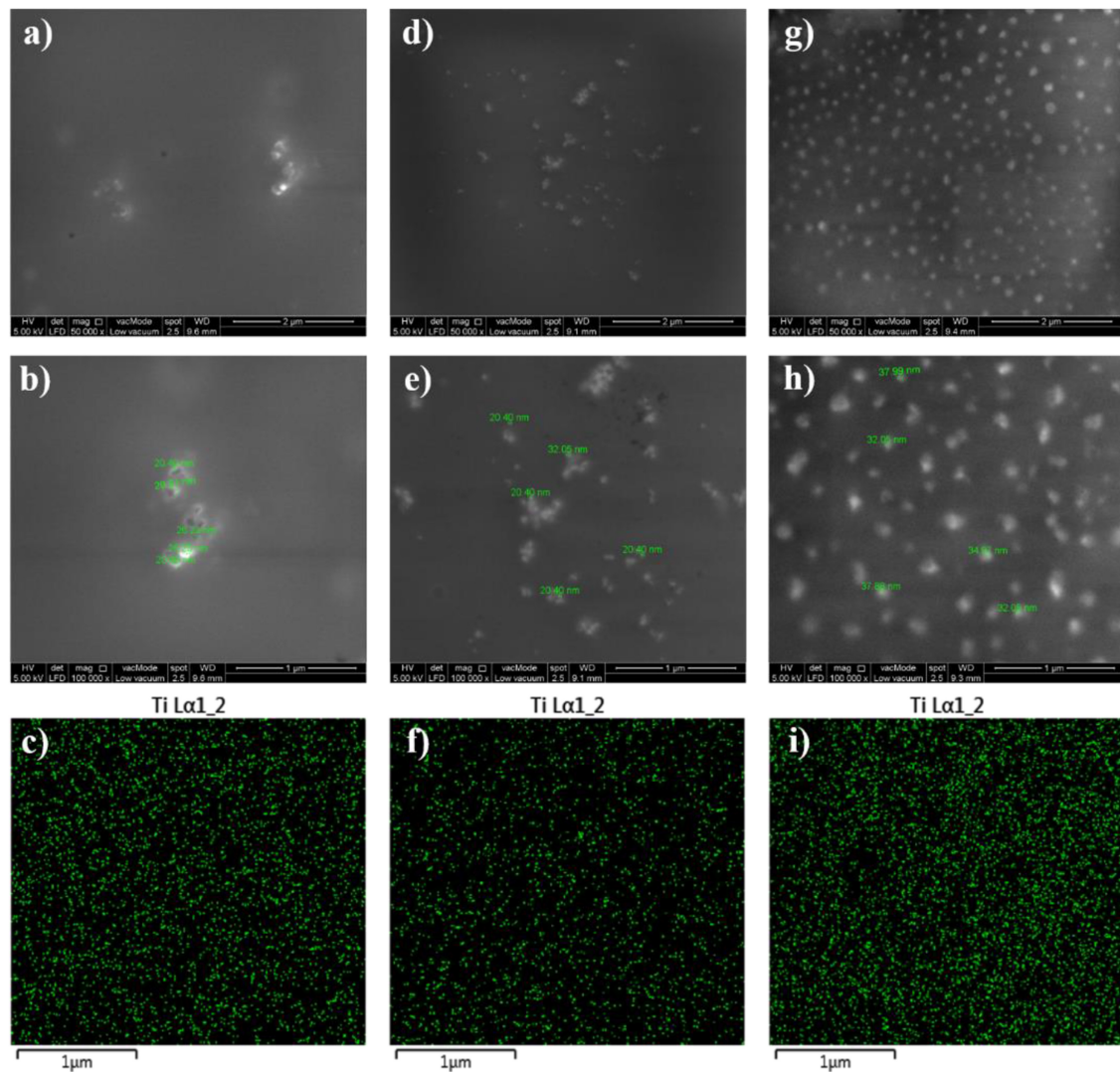
**FIGURE 3 |** FESEM images at x50000 and x100000 magnifications together with EDX mapping images for EPT1 **(a–c)**, EPT2 **(d–f)**, and EPT3 **(g–i)**.

of the epoxy coating film which led to the formation of some holes that reduces the surface evenness (Dan et al., 2018). In contrary, a significant reduction on the surface roughness was realized after the incorporation of $TiO_2$ nanoparticles within the epoxy polymeric matrix especially for 0.1 and 0.2 wt. % loading ratios. That, in turn, could be considered as strong evidence on the proper dispersion state of the nano $TiO_2$ particles and the efficiency of the sonication process in developing a good level of dispersion state and further improving the cross-linked structure by releasing the trapped solvent from the nano-polymeric blend. However, higher surface roughness was recorded with the application of the ET3 coating system due to tendency of the $TiO_2$ nanoparticles to agglomerate at the higher loading ratio, therefore, increasing the cluster size of the particles (Goyat et al., 2018).

The influences of modifying the epoxy base resin with PDMS, with and without the presence of $TiO_2$ nanoparticles, on the surface roughness of the resultant coated surfaces was also investigated by means of AFM and the findings in the form of 3 D topographical images were illustrated in **Figure 5**. Sq values of 5.8, 5.6, 4.1, and 12.6 nm were recorded for EP, EPT1, EPT2, and EPT3 coating systems, respectively. Comparing the Sq value of neat epoxy coating system, the addition of the PDMS has significantly reduced the roughness which could be corresponded to the greater level of crosslinking with the achievement of the better curing process. This observation was found in strong agreement with FTIR results and further confirm the compatibility among epoxy and PDMS resins. In the case of the addition 0.1 and 0.2. wt. % $TiO_2$ nanoparticles within the PDMS modified epoxy matrix, the AFM results did not show considerable alterations among the surface roughness which indicate the good dispersion state. However, increasing the loading ratio up to 0.3 wt. % led to change the nature of the surface toward more roughness due to the existence of a greater
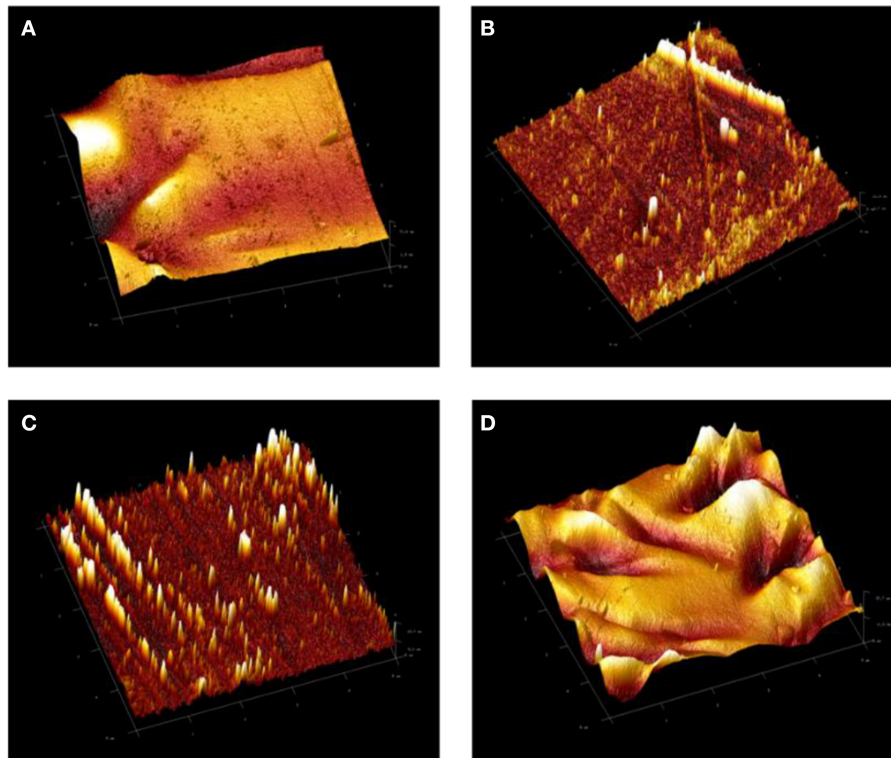
**FIGURE 4 |** 3D atomic force microscopy (AFM) images of **(A)** neat epoxy, E, coating system and **(B)** ET1, **(C)** ET2, and **(D)** ET3 epoxy-TiO$_2$ nanocomposite coating systems.

number of TiO$_2$ nanoparticles within the unit area, therefore, agglomeration formation.

## Ultraviolet-Visible (UV-Vis) Spectroscopy

Ultraviolet-visible (UV-vis) spectroscopy was used to determine the optical properties of TiO$_2$ nanoparticles within the epoxy polymeric matrix. **Figure 6** shows the UV-vis absorbance spectra of all developed coating systems. As TiO$_2$ have a wide bandgap between valence and conduction band of 3.2 eV, it tends to absorb shorter wavelength with high energy to excite its electron (Pugachevskii, 2013), typically at the UV range below 400 nm where it does not have a specific peak within this region (Gouda and Aljaafari, 2012; Karkare, 2014; Rathod and Waghuley, 2015). Therefore, when TiO$_2$ nanoparticles have been incorporated within the epoxy coating, it tends to broaden the absorption region of the epoxy and significantly enhance the existing absorption intensity at around 250 nm, which is also within the TiO$_2$ absorption range. It can be seen that the absorption at UV range is enhanced with the incorporation of TiO$_2$ nanoparticles. However, as the loading ratio of incorporated TiO$_2$ nanoparticle increased, the UV absorption intensity at around 250 nm shows a lowering trend, this is due to the fact that UV-vis absorbance highly depends on the TiO$_2$ particle size (Kormann et al., 1988; Gutierrez et al., 2008). The lowering of the absorbance intensity arises from composites' cluster morphology. The absorption intensity of all coating

system developed using epoxy-PDMS hybrid polymeric matrix namely, EP, EPT1, EPT2, and EPT3 is lower compared to neat epoxy coating. This can be attributed due to the formation of intercalation network among the two polymers and changed the conformational structure of neat epoxy coating. However, when the TiO$_2$ nanoparticles were embedded within the epoxy-PDMS hybrid matrix, broadening, and increasing of absorption intensity at the same wavelength peak observed as the amount of TiO$_2$ nanoparticles increased. This observation can further confirm that TiO$_2$ nanoparticle tends to enhance the UV absorption within their active absorption region. Due to its light-respond capability, it can be suggested on the future work that the presence of TiO$_2$ nanoparticle in coating development can improve the photogenerated cathodic protection of metals and might help from discoloration of coating product under UV illumination.

## Contact Angle (CA) Measurement

Water contact angle measurements (CA) were carried out for all prepared coating systems in order to investigate the wettability state of the developed coated surfaces and to determine the roles of the incorporated PDMS resin and the embedded TiO$_2$ nanoparticles in manipulating the wettability characters of epoxy-based coatings. **Table 2** tabulate all contact angle values with its correspondent drop image at the respective coating surfaces. The hydrophilic nature of the epoxy coatings was
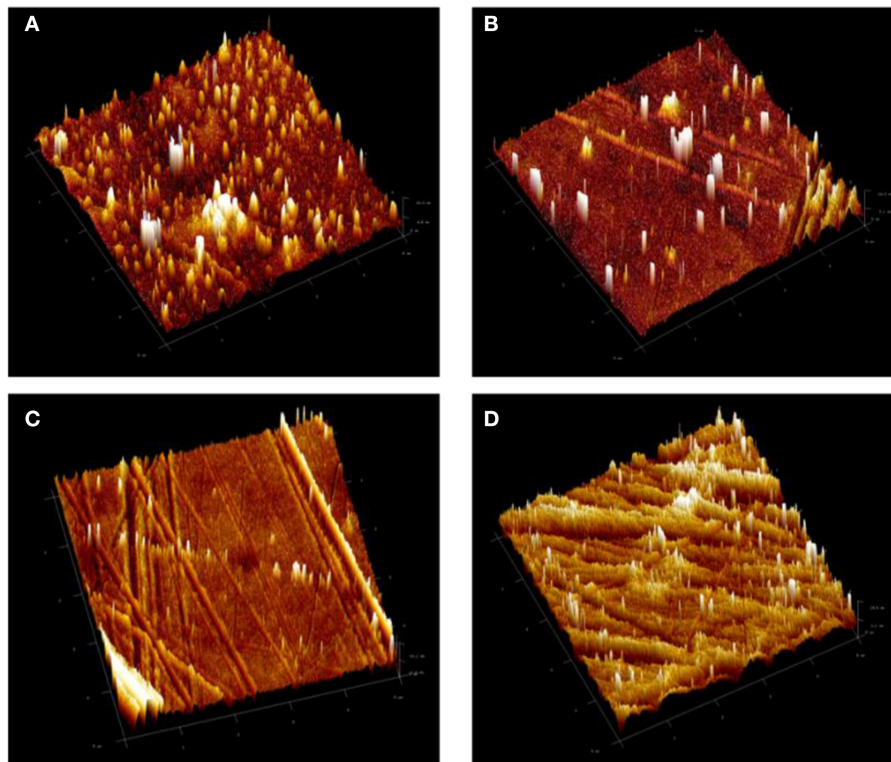
**FIGURE 5** | 3D atomic force microscopy (AFM) images of **(A)** PDMS modified epoxy, EP, coating system and **(B)** EPT1, **(C)** EPT2, and **(D)** EPT3 PDMS modified epoxy-TiO$_2$ nanocomposite coating systems.
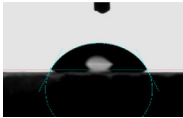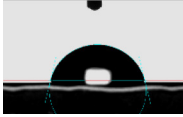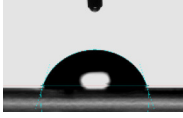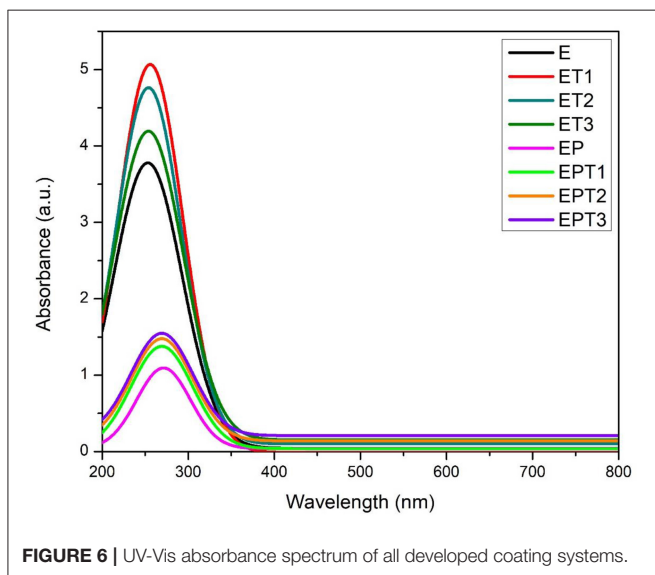


**FIGURE 6** | UV-Vis absorbance spectrum of all developed coating systems.

confirmed as the substrate coated with the E coating system demonstrated a CA value equal to ∼63°. The introducing TiO$_2$ nanoparticles within the epoxy polymeric matrix was able to enhance the wettability of the coating film toward more hydrophobicity. However, as the surface is characterized as a hydrophobic surface when the contact angle values reach

or exceed 90°, none of the utilized loading ratios of TiO$_2$ nanoparticles has resulted in that. Despite that, an increase of ∼14° in the CA values was gained by the surface coated with the ET1 coating system further confirm the excellent dispersion state of the 0.1 wt. % TiO$_2$ nanoparticles among the epoxy matrix. This observation could be attributed due to the fact that the existence of the appropriate amount of inorganic nanoparticles within the polymeric based coating system could alter the surface roughness and results in more hydrophobicity (Park et al., 2014). It was interesting to note that CA results were found to be in strong agreement with AFM findings as the substrate coated with E coating systems shows a higher value of surface roughness. This explains the lower contact value of neat epoxy coating system since the rougher surface area will lead to the spreading of the water droplet among the grooves (Asadi et al., 2019). While the incorporation of TiO$_2$ nanoparticles, with the assist of the sonication process, resulting in a lower degree of surface roughness, hence, shifting the wettability state toward more hydrophobic nature (Vázquez-Velázquez et al., 2018). It is worth mentioning that no further improvement was realized with the application of ET2 and ET3 coating systems due to the tendency of the nanoparticles at the higher loading rates to agglomerate and affect the bulk properties rather than the surface characteristics (Ramezanzadeh et al., 2011).

A hydrophobic surface was recorded after the application of EP coating with CA value almost reached 100°. This

**TABLE 2 |** The water contact angle values of all developed coating systems.

| System | Contact angle ($\theta°$) | Drop image |
|--------|---------------------------|------------|
| E | $62.9 \pm 0.5$ | |
| ET1 | $77.1 \pm 0.7$ | |
| ET2 | $72.2 \pm 0.4$ | |
| ET3 | $69.6 \pm 0.4$ | |
| EP | $99.7 \pm 0.5$ | |
| EPT1 | $103.2 \pm 0.3$ | |
| EPT2 | $100.9 \pm 0.4$ | |
| EPT3 | $98.2 \pm 0.3$ | |



**FIGURE 7 |** The equivalent circuit models used to perform the fitting for EIS graphs and **(A,B)** represent the designations of the models that used.

result was in complete agreement with finding reported by many researchers who proved the ability of PDMS resin to enhance the hydrophobicity of epoxy coatings due to its low surface energy (Eduok et al., 2017). The highest CA value obtained by EPT1 coating system which further confirms the compatibility among the coating components, the good cross-linked structure of the coating film and proper dispersion of $TiO_2$ nanoparticles with the hybrid epoxy-PDMS polymeric matrix.

## Electrochemical Impedance Spectroscopy (EIS)

Electrochemical impedance spectroscopy was performed to investigate the effects of adding different loading ratios of $TiO_2$ nanoparticles on the barrier properties and the corrosion protection performance of the epoxy-based coating systems. Moreover, EIS was also utilized to investigate the role of PDMS in improving the electrochemical behavior
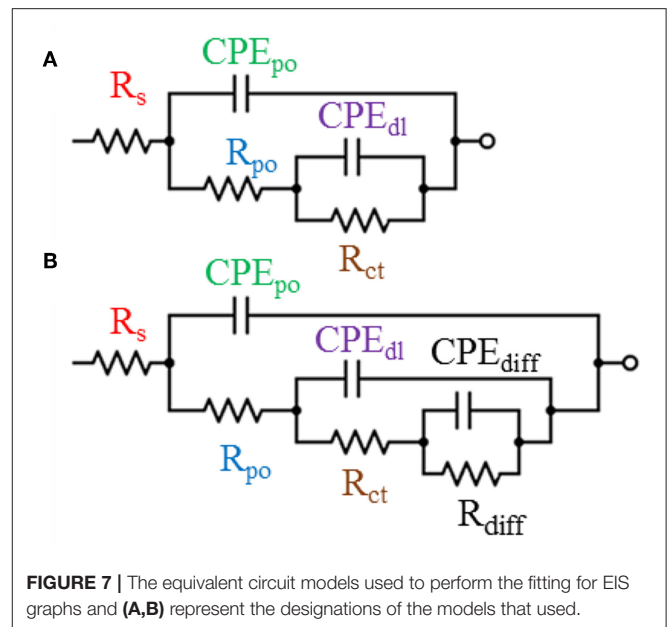
of epoxy coating and epoxy-$TiO_2$ nanocomposite coating against corrosion. After exposing the coated samples to 3.5% NaCl solution, the EIS measurements were carried out periodically and the collected results were presented graphically with Bode and Nyquist plots after 1 and 30 days of immersion time.
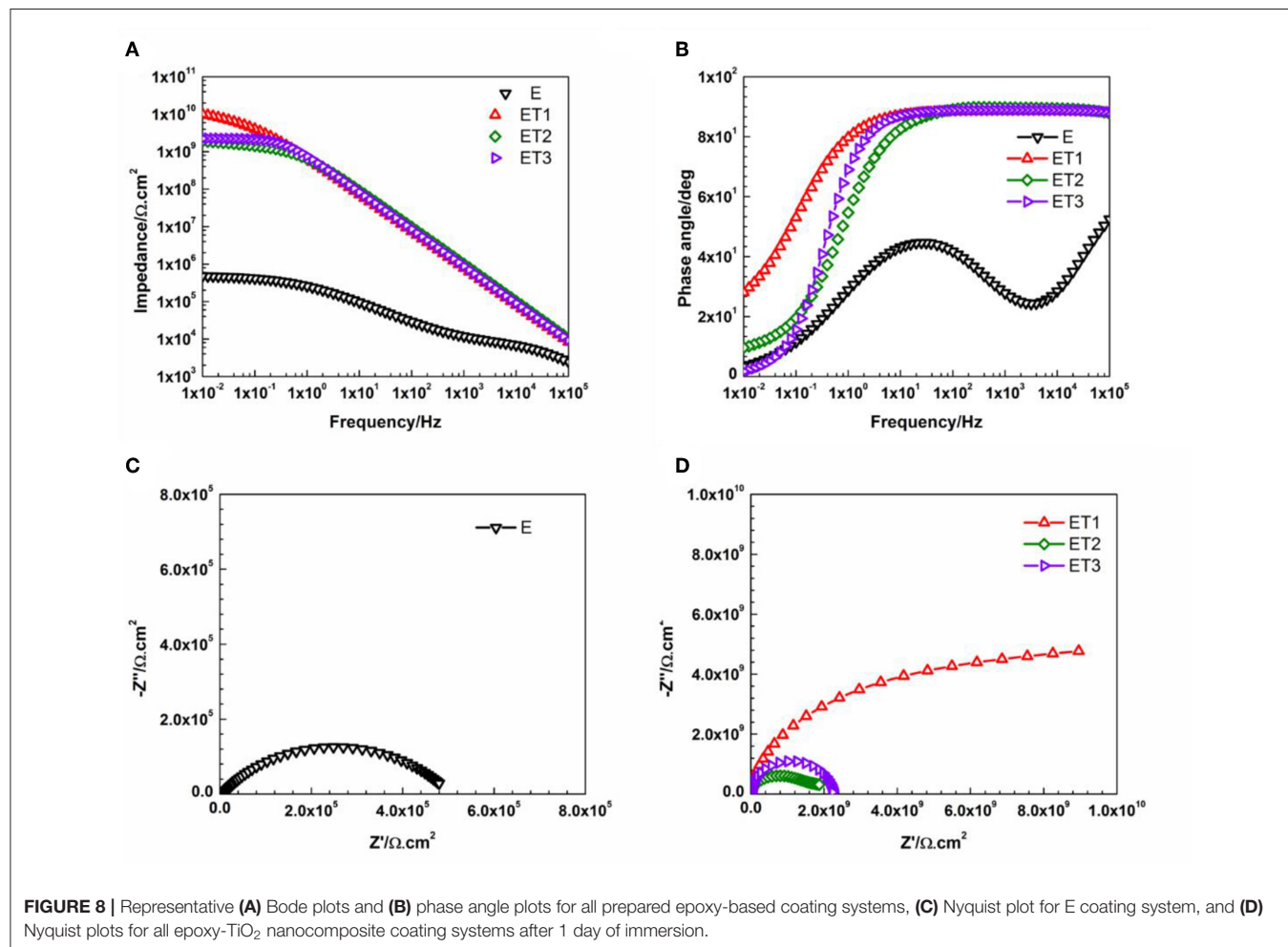
To explain the electrochemical behavior of all developed coating systems after different periods of immersion time, two models of the equivalent circuits were utilized and illustrated in **Figure 7**. As the exposure time elapsed, the electrolyte attempted to penetrate through the coating film toward the coating—substrate interface causing the initiation of the corrosion reaction. However, the corrosion protection obtained by the coating film at this stage could be understood by analyzing the electrochemical response with the assist of Model A of the equivalent circuit which composes of the following elements: a resistor Rpo and a constant phase element (CPEpo), which describes the electrolyte resistance through the film pores, and its associated (CPEpo). Also, this model includes a parallel combination of a resistor which represents the charge transfer resistance (Rct) and constant phase element as the double layer capacitance (CPEdl). The aforementioned components represent the resistance obtained by the coating film against the corrosion reaction. In order to distinguish the coating systems that are unable to withstand corrosion and failed in isolating the substrate's surface to be in direct contact with the penetrated electrolyte, Model B of the equivalent circuit was introduced. In addition to the previous elements that used to build up Model A, new constant phase element and resistor were added to Model B namely constant phase element of corrosion products diffusion capacitance (CPEdiff) and corrosion products diffusion resistance (Rdiff). Hence, by mean of Model B, the resistance obtained by the coating film against the diffusion of the corrosion

products from the substrate active sites at the coating-substrate interface could be represented. It is worth mentioning that both proposed equivalent circuit models include a resistor element Rs which serves as the solution resistance and had no significant technical or theoretical information about the developed coating systems, therefore, it was not included in this study (Ammar et al., 2016c).

Figure 8 illustrates the Bode and Nyquist plots for neat epoxy and all developed epoxy-TiO$_2$ nanocomposite coating systems after 1 day of immersion time. Even after this short period of exposure, the poor barrier properties and weak corrosion protection performance was obvious for E coating system as two-time constants and corresponded two semicircles was observed in Bode and Nyquist pots, respectively. Model B of the equivalent circuit was found to obtain the best numerical fitting for the EIS data which further indicates the initiation of the corrosion process and the formation of the corrosion products that cause the delamination of the coating film from the metal substrate. Similar observations were published by Pourhashem et al., who have investigated the corrosion protection performance of epoxy-based coating systems applied to mild steel substrates. The reported results indicate the poor barrier properties of neat epoxy coating system after only 1 day of exposure time to 3.5%

NaCl electrolyte even when it is applied at a larger thickness up to $150 \pm 10\,\mu m$ (Pourhashem et al., 2017). Moreover, the weak corrosion protection performance of epoxy based coating systems after such a short period of immersion time was reported by several researchers who studied the performance of neat epoxy coating films that applied with different thickness specifically at $120\,\mu m$ (Chang et al., 2014), $130\,\mu m$ (Li et al., 2015), and $250\,\mu m$ (Wang et al., 2018).
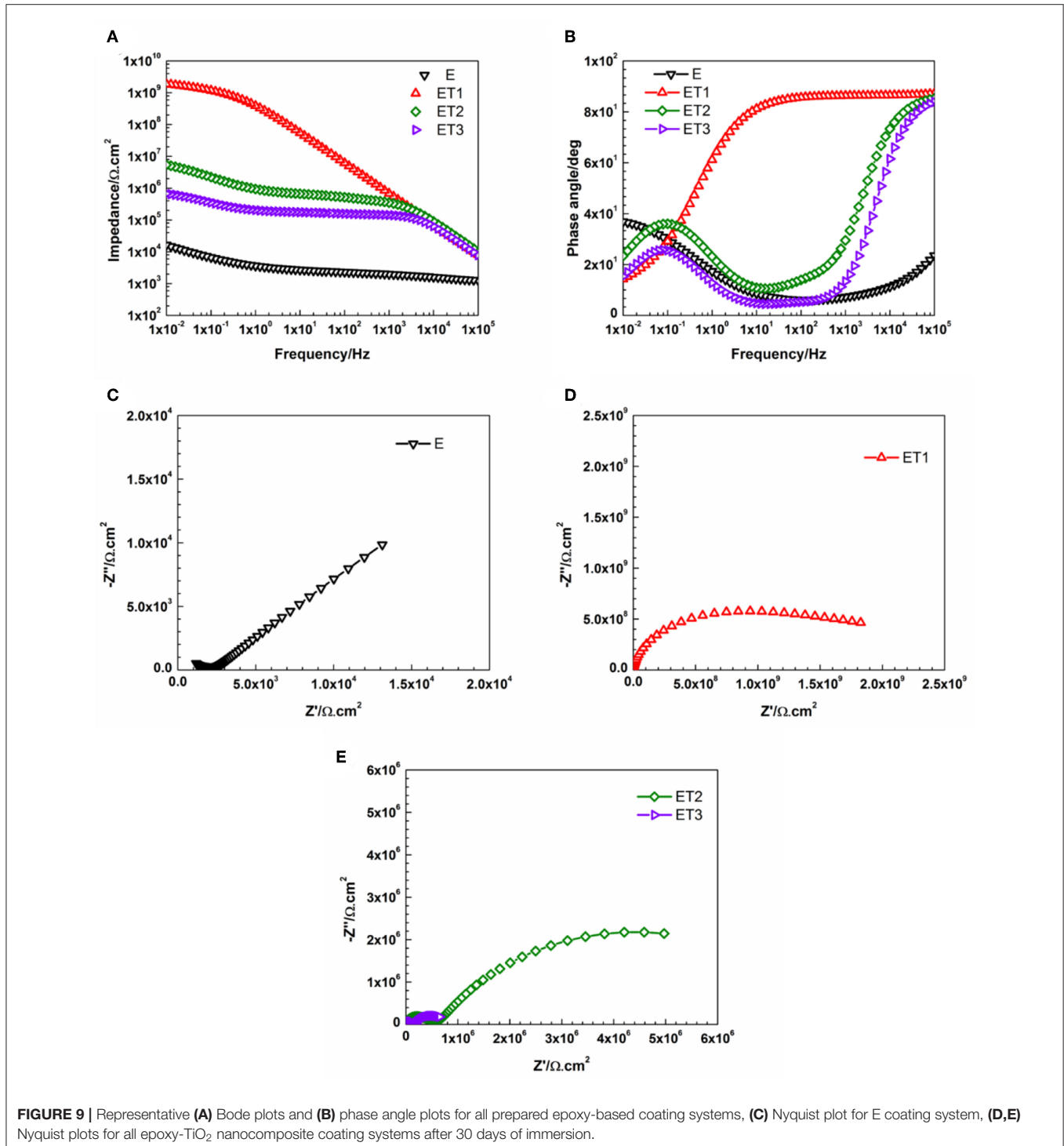
However, the incorporation of different loading rates of TiO$_2$ nanoparticles within the epoxy polymeric matrix has significantly enhanced the barrier properties of the coating films as only a slight bending of the Bode plots at the low-frequency region, as well as, one semicircle in the Nyquist plots which both fitted with model A of the equivalent circuit. These findings could be attributed to the vital role of the incorporated TiO$_2$ nanoparticles in modifying the network structure of the epoxy polymeric matrix where the embedded nanoparticles contributed in reorganizing the polymeric matrix by the physical interactions due to Van Der Waal's force that helps in closing up the pores of the epoxy matrix, hence, forcing the penetrated electrolyte to travel a longer distance in order to reach the substrate surface and lead to the corrosion reaction initiation (Ramezanzadeh et al., 2016b; Basiru et al., 2018). However, as the immersion



FIGURE 8 | Representative (A) Bode plots and (B) phase angle plots for all prepared epoxy-based coating systems, (C) Nyquist plot for E coating system, and (D) Nyquist plots for all epoxy-TiO$_2$ nanocomposite coating systems after 1 day of immersion.

time elapsed and reached 30 days, only ET1 coating system which loading with 0.1 wt. % of $TiO_2$ nanoparticles manage to obtain performance stability and perfectly protect the steel substrate from being corroded. The observation of Bode and Nyquist plots of ET1 coating systems, illustrated in **Figure 9**, interestingly demonstrated no changes over the immersion time period and still holding the ability to be fitted by means of

Model A of the equivalent circuit. This, in turn, implied that this small amount of $TiO_2$ nanoparticles was sufficient to enhance the overall performance of the coating film as the EIS finding was in strong agreement with all previously reported results.

On the other hand, all other developed coating systems namely, E, ET2, and ET3, failed to obtain the desired protection performance against corrosion as two-time constants in Bode



**FIGURE 9 |** Representative **(A)** Bode plots and **(B)** phase angle plots for all prepared epoxy-based coating systems, **(C)** Nyquist plot for E coating system, **(D,E)** Nyquist plots for all epoxy-$TiO_2$ nanocomposite coating systems after 30 days of immersion.

plots and two semicircles in Nyquist plots were observed and Model B of the equivalent circuit was utilized to obtain the fitting. The poor corrosion protection performance of E coating system could be attributed to the weak barrier properties of the epoxy polymeric matrix due to the presence of voids at the coating film surface and pores through the bulk structure of the coating layer. Yi et al. (2018) reported that the creation of the voids and the pores is due to the evaporation of the solvent during the curing process and the shrinkage of the coating layer. Moreover, the existence of these pores increases the free volume within the epoxy polymeric matrix and consider the main responsible of the creation of the diffusion pathways that permit the corrosive agents to penetrate through the coating

film, hence, the degradation of the corrosion protection ability (Ramezanzadeh et al., 2016a). The most pronounced effect of $TiO_2$ nanoparticles was realized with its loaded at 0.1 wt. %, within ET1 coating system. That could be attributed to the proper dispersion of the nano reinforcing agents within the polymeric matrix, hence, reducing the porosity and zigzagging the diffusion pathway. However, the EIS findings revealed that the further addition of $TiO_2$ nanoparticles did not significantly enhance the corrosion protection performance of the polymeric matrix. The 2016 work of Kumar et al., discuss the effects of different concentrations of $TiO_2$ nanoparticles on the epoxy matrices and have concluded that the higher loading ratios of $TiO_2$ could affect its dispersion state and led to the formation of larger
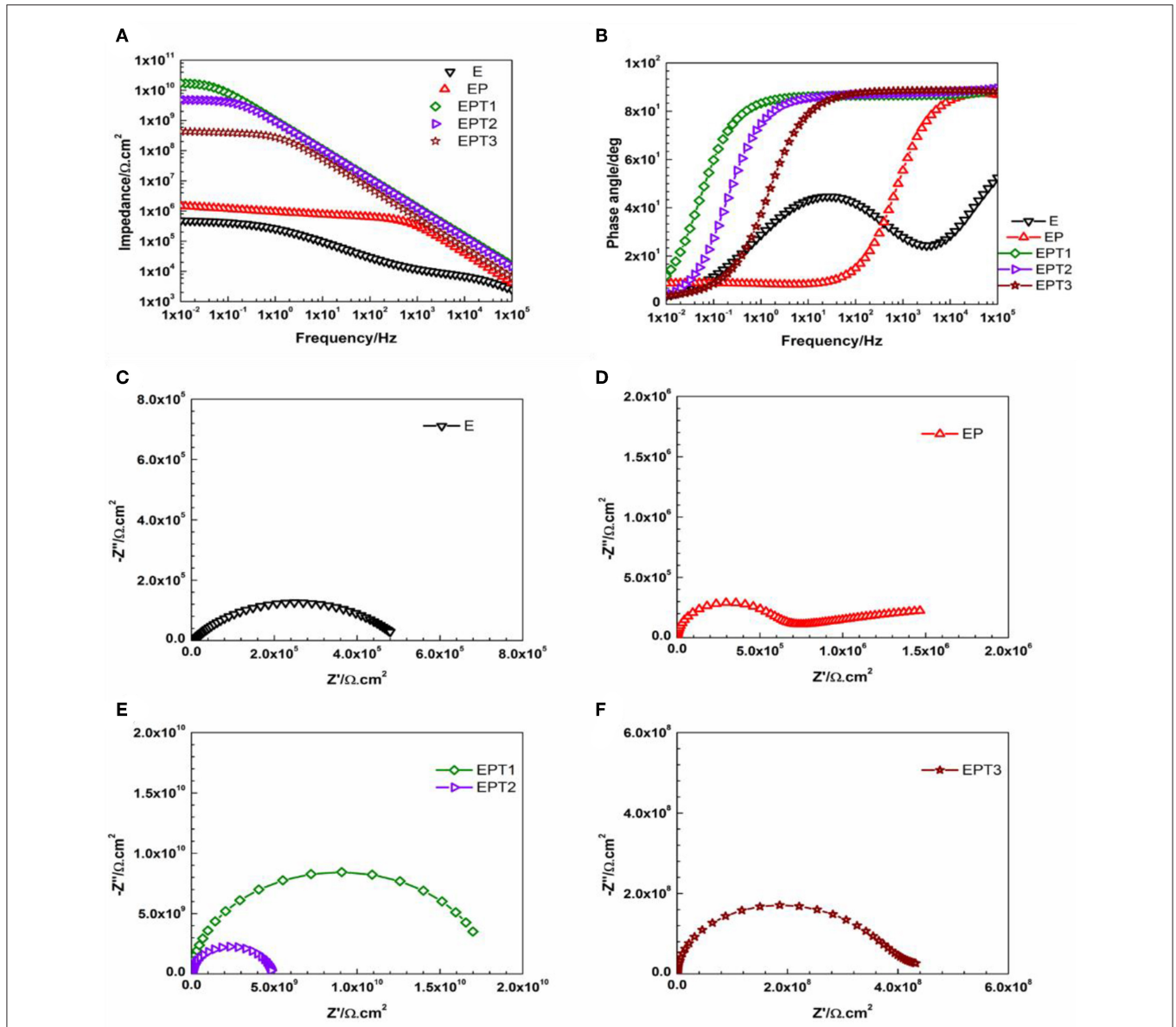


**FIGURE 10 |** Representative **(A)** Bode plots and **(B)** phase angle plots for E, EP, and all PDMS modified epoxy nanocomposite coatings, and Nyquist plots for **(C)** E, **(D)** EP, **(E)** EPT1 and EPT2, **(F)** EPT3 coating systems after 1 day of immersion.

clusters, hence, alter the contact among the nanoparticles and the epoxy matrix and narrow their interaction that is essential for the interfacial adhesion (Kumar et al., 2016). Furthermore, the numerical values of all parameters that have been obtained by fitting the EIS data of E coating system and all epoxy-TiO$_2$ nanocomposite coating systems after 1 and 30 days of immersion time with its respective equivalent circuit models were tabulated in **Tables S1, S2**, respectively.

Recently, several studies confirmed the development of better corrosion protection performance of polymeric based coating systems that possess hydrophobic nature (Huang et al., 2019; Zhang et al., 2019; Zhu et al., 2019). Therefore, the wettability of the developed coated surfaces become to be considered as
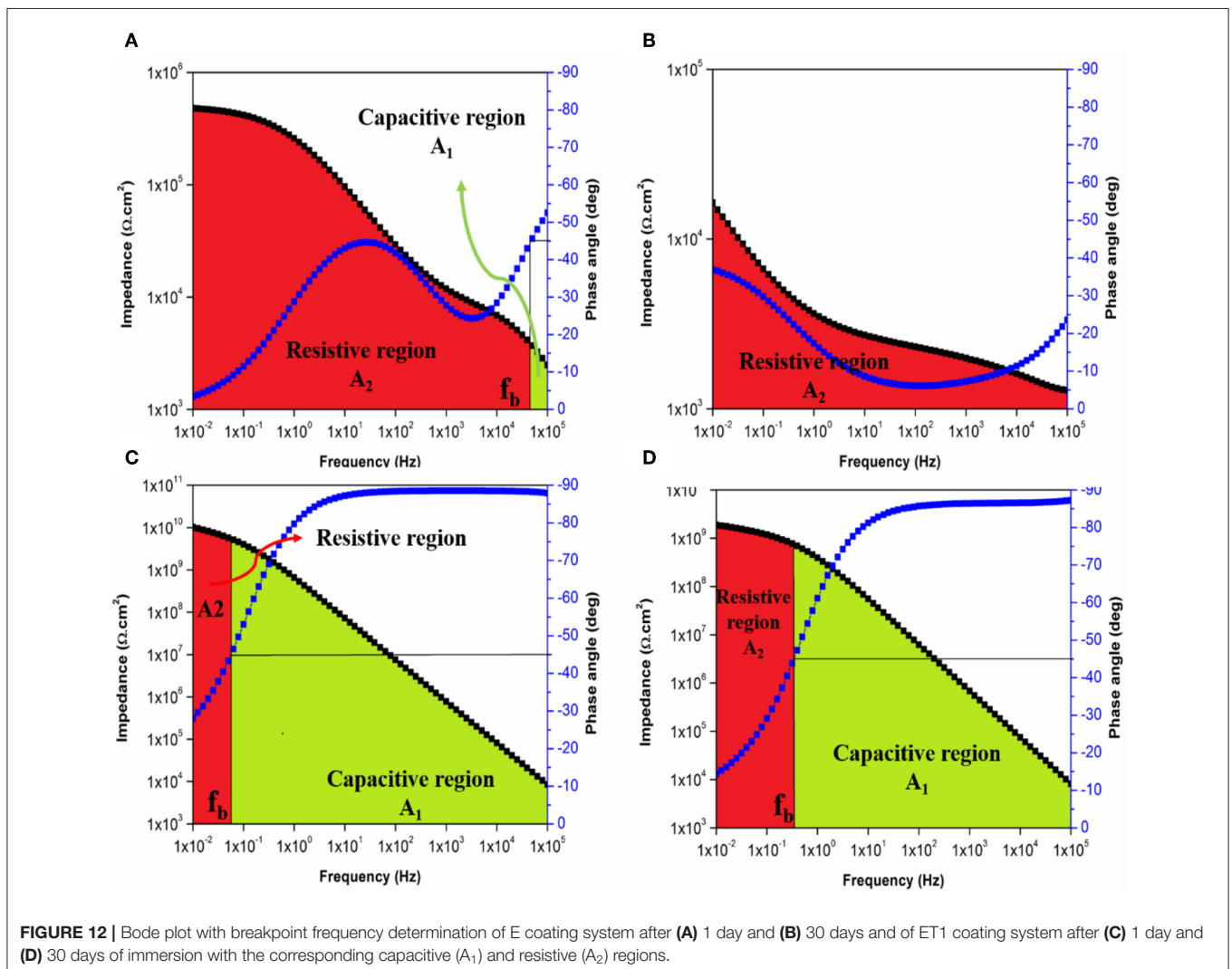
one of the indicators about the corrosion protection ability of the coating system. In this study, attempts have been made to enhance the hydrophobicity by modifying the epoxy base resin with PDMS. From **Figures 10**, **11**, which represent the Bode and Nyquist plots of E, EP and all PDMS modified epoxy nanocomposite coating systems after 1 and 30 days of immersion time, respectively, it can be seen that utilizing PDMS resin as a modifier have enhanced the barrier properties of the coating film and ensure the performance stability of the coating system over the whole periods of immersion time. Even though the EIS data for EP coating system was found to be perfectly fitted with Model A of the equivalent circuit after 1 and 30 days of immersion time, but the bending of



**FIGURE 11 |** Representative **(A)** Bode plots and **(B)** phase angle plots for E, EP, and all PDMS modified epoxy nanocomposite coatings, and Nyquist plots for **(C)** E, **(D)** EP, EPT2, and EPT3, **(E)** EPT1 coating systems after 30 days of immersion.
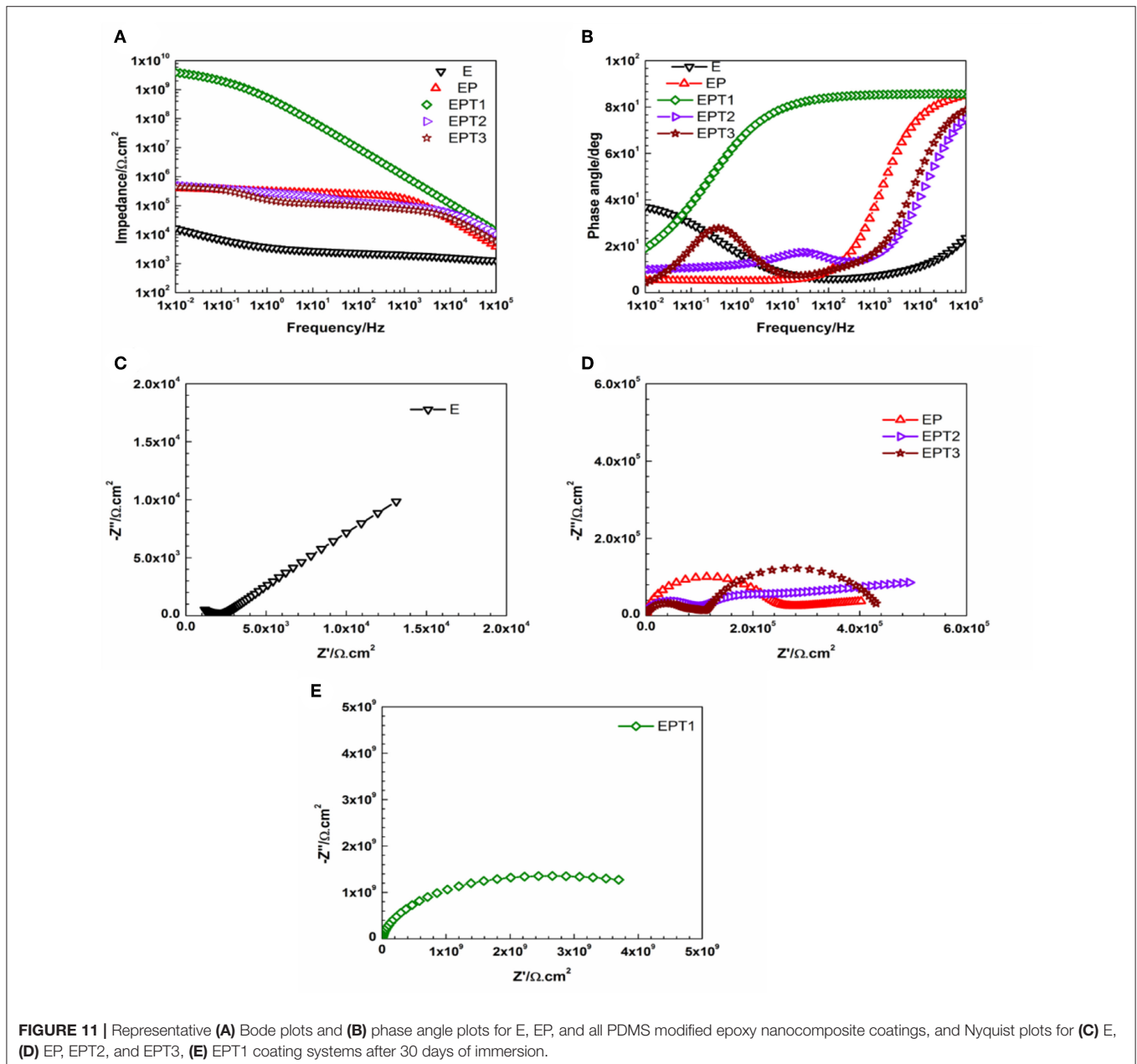
the Bode plot at the high-frequency region and the small diameter of the semicircle in the Nyquist plot indicate a fair corrosion ability. Similar observations were reported by Ammar et al. who utilized the breakpoint frequency concept to the analysis the stability of the epoxy-PDMS hybrid coating system and concluded with that fact that as the immersion time elapsed, larger resistive region and relatively smaller capacitive region are observed in the area under the Bode plot which resulted from the shifting of the breakpoint frequency values toward the higher frequencies region, hence a reduction of the barrier properties of the coating film is occurring (Ammar et al., 2017).

Among all developed EP nanocomposite coating systems, the most pronounced enhancement was recorded for EPT1 coating system as a Bode plot with slight bending at the low-frequency region and Nyquist plot with one semicircle after 1 and 30 days of immersion time indicate the capacitive behavior and the stability of the coating film over the whole period of exposure without any significant signs for coating deterioration or loss of the intact barrier properties. Model A of the equivalent

circuit was used to obtain the numerical fitting for both EIS graphs after 1 and 30 days of immersion time. Furthermore, it was interesting to notice that 0.1 wt. % of $TiO_2$ nanoparticles was found to be the optimum loading ratio that results in the best corrosion protection performance for both utilized polymeric matrices namely, neat epoxy and PDMS modified epoxy matrix. Apart from that, more stability against corrosion was realized for EPT1 coating system with higher impedance values over the whole periods of immersion. This could be attributed due to the role of the PDMS modifier in obtaining the hydrophobicity to the coating film. The relation among the hydrophobic character of the coated surface and its barrier properties could be explained as increasing the hydrophobicity will lead to minimizing the areas of the surface that are in direct contact with the aqueous electrolyte solution, hence, reducing the electrolyte absorption within the coating film and enhance its barrier properties. Moreover, the existence of good dispersed $TiO_2$ nanoparticles within the PDMS modified epoxy marix magnified the protection obtained by the coating film against the pentation of the electrolyte toward the coating—substrate



**FIGURE 12** | Bode plot with breakpoint frequency determination of E coating system after **(A)** 1 day and **(B)** 30 days and of ET1 coating system after **(C)** 1 day and **(D)** 30 days of immersion with the corresponding capacitive ($A_1$) and resistive ($A_2$) regions.
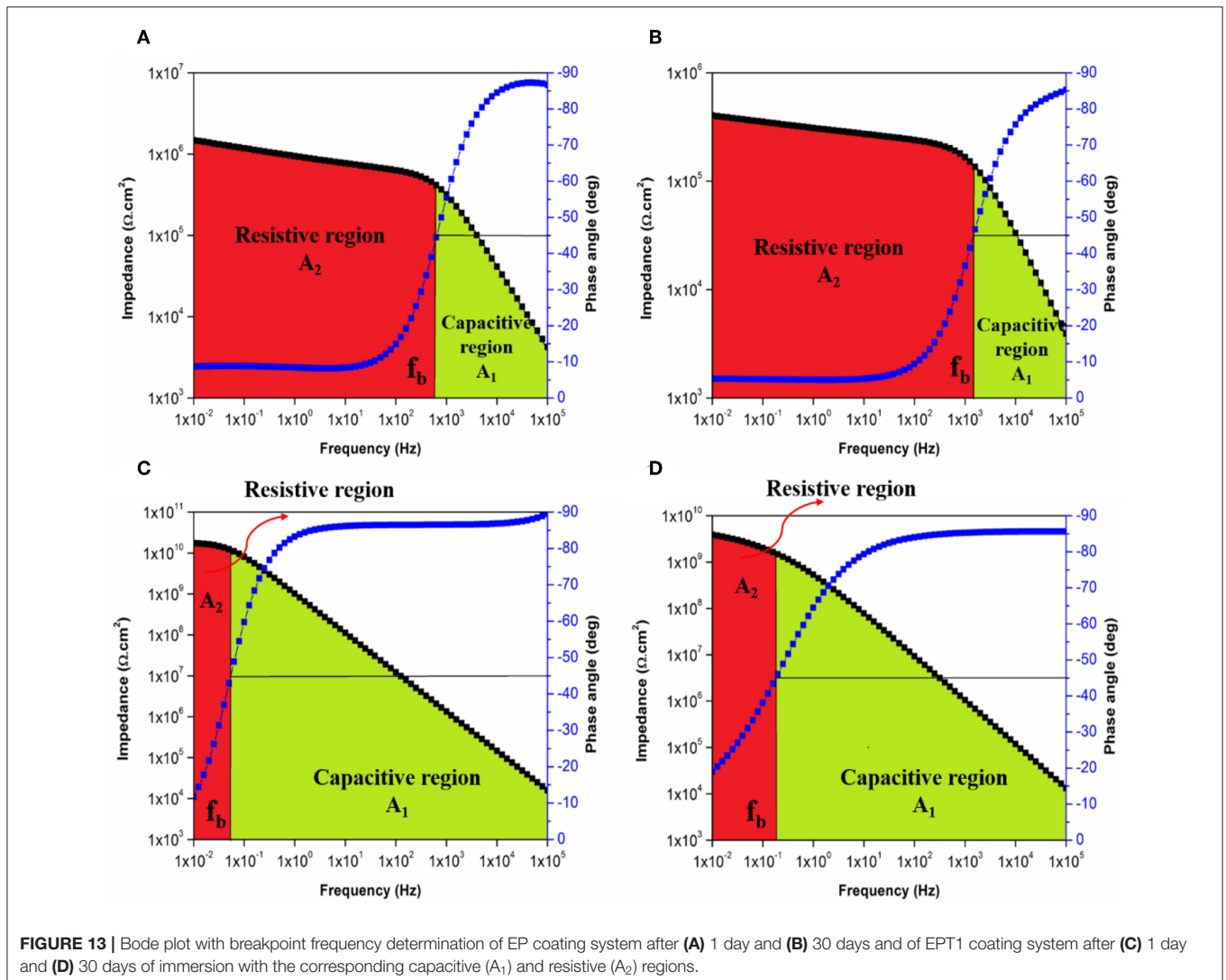
interface by filling up the matrix pores and zigzagging the diffusion pathways (Ammar et al., 2016a). However, as in epoxy-TiO$_2$ nanocomposites that mentioned above, further increasing the loading ratio of TiO$_2$ nanoparticles up to 0.2 and 0.3 wt. % did not show any additional improvement to the corrosion protection performance which could also attributed to the tendency of the nanoparticles to agglomerate at the high loading ratios. Furthermore, the numerical values of all parameters that have been obtained by fitting the EIS data of E, EP, and all PDMS modified epoxy nanocomposite coating systems after 1 and 30 days of immersion time with its respective equivalent circuit models were tabulated in **Tables S3, S4**, respectively.

In the ideal coating system, the applied layer covers the enter surface area of the specimen and acts as a perfect capacitor. However, as the electrolyte penetrates and reaches the substrate, it tends to settle in the microporous at the coating-substrate interface and leads to promote the corrosion process. Hence, the performance at these spots is considered

as a resistive behavior. Therefore, analyzing the areas under the bode plot and its interpretations, with the assist of breakpoint frequency values, could play a vital role in obtaining a better understanding of corrosion processes at the coating—substrate interfaces and its implications for film delamination and loss of adhesion that lead to the degradation of the protection system. Zhang et al. (2007) have investigated the delamination of TiO$_2$-epoxy nanocomposite coating system based on the relation suggested by Hirayama and Haruyama (1991):

$$f_b = \frac{S}{2\pi\varepsilon\rho} \tag{1}$$

Where, S is the ratio of delaminated area to the original area, $\rho$ is the coating resistivity and $\varepsilon$ is the dielectric constant. Hence, the breakpoint frequency and its changes over the different period of immersion time for a giving coating system is proportional to the delaminated area. To that end, the impedance and phase angles values were plotted



**FIGURE 13 |** Bode plot with breakpoint frequency determination of EP coating system after **(A)** 1 day and **(B)** 30 days and of EPT1 coating system after **(C)** 1 day and **(D)** 30 days of immersion with the corresponding capacitive (A$_1$) and resistive (A$_2$) regions.

as functions to their frequencies. After that, the intersection of the breakpoint frequency ($f_b$), which is defined as the frequency at $45°$ phase angle, with the impedance curve was considered to distinguish the different areas under the Bode plots.

With respect to the immersion time, the performance of the applied coatings could be evaluated based on the regions under the Bode plot. An intact character of the coating system is realized when the phase angle remains higher than $45°$ over the whole tested frequency range the area under the Bode plot is recognized as a capacitive region. While in the case of observing two areas under the Bode plot namely, capacitive and resistive regions, coating film undergoing corrosion is considered (Javidparvar et al., 2019). The failure of the coating system is confirmed when only a resistive region is observed below the Bode plot. **Figures 12A–D** illustrate the areas under Bode plot for E and ET1 coating systems based on its $f_b$ values after 1 and 30 days of immersion. While the plots of ET2 and ET3 were illustrated in **Figures S9, S10**. **Figure 12A** shows both capacitive and resistive areas under the Bode plot of the E coating system after 1 day of immersion time. As the immersion time elapsed, only the resistive region was observed in **Figure 12B** which further indicates the poor corrosion protection performance of neat epoxy coating system. Apart from that, the incorporation 0.1 wt. % of $TiO_2$ nanoparticles within the epoxy polymeric matrix has significantly enhanced the barrier properties of the coating film as the lower value of breakpoint frequency was recorded, hence, relatively smaller resistive regions in the low-frequency range and larger capacitive regions are observed in **Figures 12C,D**. No further improvement was realized with increasing the $TiO_2$ concentrations within the epoxy polymeric matrix as higher $f_b$ values and increased size of the resistive regions over the capacitive regions were recorded in **Tables S1, S2** and **Figures S11, S12**.

In the same manner, the influences of PDMS on the $TiO_2$-epoxy nanocomposite coating systems were discussed by means of breakpoint frequencies and the areas under Bode plots were illustrated in **Figures 13A–D** for EP and EPT1 coating systems. Whereas, **Figures S11, S12** show the areas under bode plots of EPT2 and EPT3, respectively. Comparing to the neat epoxy coating system, modifying the epoxy resin with PDMS has resulted in shifting the $f_b$ values toward the lower frequency region, therefore, increases the size of the capacitive region over the resistive region as observed in **Figures 13A,B**. The most pronounced improvement was realized, in **Figure 13C**, for EPT1 coating system as the lowest $f_b$ values, the largest capacitive region and smallest resistive region were recorded after 1 day of immersion time. Moreover, the remarkable stability of the aforementioned coating system against the initiation of corrosion whereby the coating layer successfully prevented the penetration of corrosive agents was confirmed due to the non-significant changes in the $f_b$ values up to 30 days of immersion time. However, no further improvement was recorded as the loading ratio of $TiO_2$ nanoparticles reached 0.2 and 0.3 wt. % due to

the tendency of the nanoparticles to agglomerate and form larger clusters.

## CONCLUSION

Different loading ratios of $TiO_2$ nanoparticles were introduced within epoxy resin by the utilization of the solution intercalation method with the presence of the sonication process. Several characterization techniques were employed to evaluate the overall performance of the developed nanocomposite coating systems. FTIR and DSC results revealed the achievement of proper crosslinked structure of the epoxy-based coating systems with the presence of cycloaliphatic amine curing agent and the observation of single glass transition temperature in all recorded thermographs. Moreover, the dispersion state of $TiO_2$ nanoparticles within the epoxy was investigates by FESEM and EDX. The Findings confirmed the efficiency of the sonication process and room temperature curing process in achieving good desperation of $TiO_2$ nanoparticles especially when it is loaded at 0.1 wt. %. The incorporation of $TiO_2$ nanoparticles demonstrated a photocatalytic effect on the coating film as increased the absorbance at UV region. Lower surface roughness, higher CA values and better corrosion protection performance were recorded for all $TiO_2$ nanocomposite coating systems and the most pronouncing effect was realized with the utilization of 0.1 wt. % loading ratio. The reported finding revealed the compatibility of $TiO_2$ nanoparticles to be embedded within the epoxy matrix and its ability to physically interact with the epoxy network resulting in high $T_g$ values and better barrier properties via reducing the porosity and zigzagging the diffusion pathway of the polymeric matrix. Furthermore, PDMS resin was used to modified the epoxy-based resin and the hybrid polymeric matric was used to host different loading ratio of $TiO_2$ nanoparticles. Similiter to epoxy-$TiO_2$ nanocomposites, good curing level with proper dispersion state of $TiO_2$ nanoparticles were recorded with the presence of PDMS modifier. The low surface energy of PDMS resin led to alter the wettability of the epoxy resin toward more hydrophobic character. Moreover, 0.1 wt. % of $TiO_2$ nanoparticles was also confirmed to be the optimum concentration that significantly enhanced the barrier properties and corrosion protection ability of the coating film. Therefore, PDMS resin was confirmed to be a suitable modifier that is able to enhance the hydrophobicity of the resulting coated surfaces without alter the curing level, glass transition temperature, dispersion state and the corrosion protection performance of $TiO_2$-epoxy nanocomposite coating systems.

## DATA AVAILABILITY STATEMENT

All datasets generated for this study are included in the article/**Supplementary Material**.

## AUTHOR CONTRIBUTIONS

AS, CC, and IW prepared the samples, carried out the characterizations, data analysis, and wrote the manuscript. SB

and VB assisted in performing the tests and data analysis. RK and RS supervised the overall research work and finalized the manuscript.

## REFERENCES

Ahmad, S., Gupta, A., Sharmin, E., Alam, M., and Pandey, S. (2005). Synthesis, characterization and development of high performance siloxane-modified epoxy paints. *Prog. Org. Coat.* 54, 248–255. doi: 10.1016/j.porgcoat.2005.06.013

Ammar, S., Ramesh, K., Ma, I., Farah, Z., Vengadaesvaran, B., Ramesh, S., et al. (2017). Studies on $SiO_2$-hybrid polymeric nanocomposite coatings with superior corrosion protection and hydrophobicity. *Surf. Coat. Technol.* 324, 536–545. doi: 10.1016/j.surfcoat.2017.06.014

Ammar, S., Ramesh, K., Vengadaesvaran, B., Ramesh, S., and Arof, A. (2016a). Formulation and characterization of hybrid polymeric/ZnO nanocomposite coatings with remarkable anti-corrosion and hydrophobic characteristics. *J. Coat. Technol. Res.* 13, 921–930. doi: 10.1007/s11998-016-9799-z

Ammar, S., Ramesh, K., Vengadaesvaran, B., Ramesh, S., and Arof, A. (2016b). Amelioration of anticorrosion and hydrophobic properties of epoxy/PDMS composite coatings containing nano ZnO particles. *Prog. Org. Coat.* 92, 54–65. doi: 10.1016/j.porgcoat.2015.12.007

Ammar, S., Ramesh, K., Vengadaesvaran, B., Ramesh, S., and Arof, A. (2016c). A novel coating material that uses nano-sized $SiO_2$ particles to intensify hydrophobicity and corrosion protection properties. *Electrochim. Acta* 220, 417–426. doi: 10.1016/j.electacta.2016.10.099

Ansari, F., Galland, S., Johansson, M., Plummer, C. J., and Berglund, L. A. (2014). Cellulose nanofiber network for moisture stable, strong and ductile biocomposites and increased epoxy curing rate. *Compos. Part A* 63, 35–44. doi: 10.1016/j.compositesa.2014.03.017

Asadi, F., Jannesari, A., and Arabi, A. (2019). Epoxy siloxane/ZnO quantum dot nanocomposites: Model-fitting and model-free approaches to kinetic analysis of non-isothermal curing process. *Progr. Org. Coat.* 135, 270–280. doi: 10.1016/j.porgcoat.2019.06.006

Atta, A. M., Mohamed, N. H., Rostom, M., Al-Lohedan, H. A., and Abdullah, M. M. (2019). New hydrophobic silica nanoparticles capped with petroleum paraffin wax embedded in epoxy networks as multifunctional steel epoxy coatings. *Prog. Org. Coat.* 128, 99–111. doi: 10.1016/j.porgcoat.2018.12.018

Basiru, Y., Ammar, S., Ramesh, K., Vengadaesvaran, B., Ramesh, S., and Arof, A. (2018). Corrosion protection performance of nanocomposite coatings under static, UV, and dynamic conditions. *J. Coat. Technol. Res.* 15, 1035–1047. doi: 10.1007/s11998-017-0038-z

Brusciotti, F., Snihirova, D. V., Xue, H., Montemor, M. F., Lamaka, S. V., and Ferreira, M. G. (2013). Hybrid epoxy–silane coatings for improved corrosion protection of Mg alloy. *Corros. Sci.* 67, 82–90. doi: 10.1016/j.corsci.2012.10.013

Chang, K.-C., Hsu, M.-H., Lu, H.-I., Lai, M.-C., Liu, P.-J., Hsu, C.-H., et al. (2014). Room-temperature cured hydrophobic epoxy/graphene composites as corrosion inhibitor for cold-rolled steel. *Carbon* 66, 144–153. doi: 10.1016/j.carbon.2013.08.052

Dan, S., Gu, H., Tan, J., Zhang, B., and Zhang, Q. (2018). Transparent epoxy/TiO2 optical hybrid films with tunable refractive index prepared via a simple and efficient way. *Prog. Org. Coat.* 120, 252–259. doi: 10.1016/j.porgcoat.2018.02.017

Dolatzadeh, F., Moradian, S., and Jalili, M. M. (2011). Influence of various surface treated silica nanoparticles on the electrochemical properties of $SiO_2$/polyurethane nanocoatings. *Corros. Sci.* 53, 4248–4257. doi: 10.1016/j.corsci.2011.08.036

Duraibabu, D., Ganeshbabu, T., Manjumeena, R., and Dasan, P. (2014). Unique coating formulation for corrosion and microbial prevention of mild steel. *Prog. Org. Coat.* 77, 657–664. doi: 10.1016/j.porgcoat.2013.12.002

Eduok, U., Faye, O., and Szpunar, J. (2017). Recent developments and applications of protective silicone coatings: a review of PDMS functional materials. *Prog. Org. Coat.* 111, 124–163. doi: 10.1016/j.porgcoat.2017.05.012

Evans, P., and Sheel, D. (2007). Photoactive and antibacterial TiO2 thin films on stainless steel. *Surf. Coat. Technol.* 201, 9319–9324. doi: 10.1016/j.surfcoat.2007.04.013

Fu, G., Vary, P. S., and Lin, C.-T. (2005). Anatase TiO2 nanocomposites for antimicrobial coatings. *J. Phys. Chem. B* 109, 8889–8898. doi: 10.1021/jp0502196

Gouda, M., and Aljaafari, A. I. (2012). Augmentation of multifunctional properties of cellulosic cotton fabric using titanium dioxide nanoparticles. *Adv. Nanopart.* 1, 29–36. doi: 10.4236/anp.2012.13005

Goyat, M., Rana, S., Halder, S., and Ghosh, P. (2018). Facile fabrication of epoxy-TiO2 nanocomposites: a critical analysis of $TiO_2$ impact on mechanical properties and toughening mechanisms. *Ultrason. Sonochem.* 40, 861–873. doi: 10.1016/j.ultsonch.2017.07.040

Guo, J., Yuan, S., Jiang, W., Lv, L., Liang, B., and Pehkonen, S. O. (2018). Polymers for combating biocorrosion. *Front. Mater.* 5:10. doi: 10.3389/fmats.2018.00010

Gutierrez, J., Tercjak, A., Garcia, I., Peponi, L., and Mondragon, I. (2008). Hybrid titanium dioxide/PS-b-PEO block copolymer nanocomposites based on sol–gel synthesis. *Nanotechnology* 19:155607. doi: 10.1088/0957-4484/19/15/155607

Heidarian, M., Shishesaz, M., Kassiriha, S., and Nematollahi, M. (2010). Characterization of structure and corrosion resistivity of polyurethane/organoclay nanocomposite coatings prepared through an ultrasonication assisted process. *Prog. Org. Coat.* 68, 180–188. doi: 10.1016/j.porgcoat.2010.02.006

Heidarian, M., Shishesaz, M., Kassiriha, S., and Nematollahi, M. (2011). Study on the effect of ultrasonication time on transport properties of polyurethane/organoclay nanocomposite coatings. *J. Coat. Technol. Res.* 8, 265–274. doi: 10.1007/s11998-010-9297-1

Hirayama, R., and Haruyama, S. (1991). Electrochemical impedance for degraded coated steel having pores. *Corrosion* 47, 952–958. doi: 10.5006/1.3585208

Huang, W., Xiao, Y., Huang, Z., Tsui, G. C., Yeung, K., Tang, C., et al. (2019). Super-hydrophobic polyaniline-TiO2 hierarchical nanocomposite as anticorrosion coating. *Mater. Lett.* 258:126822. doi: 10.1016/j.matlet.2019.126822

Javidparvar, A. A., Naderi, R., and Ramezanzadeh, B. (2019). Epoxy-polyamide nanocomposite coating with graphene oxide as cerium nanocontainer generating effective dual active/barrier corrosion protection. *Compos. Part B Eng.* 172, 363–375. doi: 10.1016/j.compositesb.2019.05.055

Karkare, M. M. (2014). "Estimation of band gap and particle size of TiO2 nanoparticle synthesized using sol gel technique," in *2014 International Conference on Advances in Communication and Computing Technologies ICACACT 2014* (Mumbai: IEEE), 1–5. doi: 10.1109/EIC.2015.7230747

Kormann, C., Bahnemann, D. W., and Hoffmann, M. R. (1988). Preparation and characterization of quantum-size titanium dioxide. *J. Phys. Chem.* 92, 5196–5201. doi: 10.1021/j100329a027

Kumar, K., Ghosh, P., and Kumar, A. (2016). Improving mechanical and thermal properties of TiO2-epoxy nanocomposite. *Compos. Part B Eng.* 97, 353–360. doi: 10.1016/j.compositesb.2016.04.080

Kumar, S. A., Alagar, M., and Mohan, V. (2002). Studies on corrosion-resistant behavior of siliconized epoxy interpenetrating coatings over mild steel surface by electrochemical methods. *J. Mater. Eng. Perform.* 11, 123–129. doi: 10.1361/105994902770344178

Kumar, S. A., Balakrishnan, T., Alagar, M., and Denchev, Z. (2006). Development and characterization of silicone/phosphorus modified epoxy materials and their application as anticorrosion and antifouling coatings. *Prog. Org. Coat.* 55, 207–217. doi: 10.1016/j.porgcoat.2005.10.001

Kumar, S. A., and Narayanan, T. S. (2002). Thermal properties of siliconized epoxy interpenetrating coatings. *Prog. Org. Coat.* 45, 323–330. doi: 10.1016/S0300-9440(02)00062-0

Li, P., He, X., Huang, T.-C., White, K. L., Zhang, X., Liang, H., et al. (2015). Highly effective anti-corrosion epoxy spray coatings containing self-assembled clay in smectic order. *J. Mater. Chem. A* 3, 2669–2676. doi: 10.1039/C4TA06221C

Liao, M., Schneider, A. F., Laengert, S. E., Gale, C. B., Chen, Y., and Brook, M. A. (2018). Living synthesis of silicone polymers controlled by humidity. *Eur. Polym. J.* 107, 287–293. doi: 10.1016/j.eurpolymj.2018.07.023

Liqiang, J., Xiaojun, S., Weimin, C., Zili, X., Yaoguo, D., and Honggang, F. (2003). The preparation and characterization of nanoparticle TiO2/Ti films and their photocatalytic activity. *J. Phys. Chem. Solids* 64, 615–623. doi: 10.1016/S0022-3697(02)00362-1

Ma, I. W., Sh, A., Ramesh, K., Vengadaesvaran, B., Ramesh, S., and Arof, A. (2017). Anticorrosion properties of epoxy-nanochitosan nanocomposite coating. *Prog. Org. Coat.* 113, 74–81. doi: 10.1016/j.porgcoat.2017.08.014

Matin, E., Attar, M., and Ramezanzadeh, B. (2015). Investigation of corrosion protection properties of an epoxy nanocomposite loaded with polysiloxane surface modified nanosilica particles on the steel substrate. *Prog. Org. Coat.* 78, 395–403. doi: 10.1016/j.porgcoat.2014.07.004

Mohamad Saidi, N., Shafaamri, A. S., Wonnie Ma, I. A., Kasi, R., Balakrishnan, V., and Subramaniam, R. (2018). Development of anti-corrosion coatings using the disposable waste material. *Pigment Resin Technol.* 47, 478–484. doi: 10.1108/PRT-03-2018-0030

Moura, J. H. L., Heinen, M., da Silva, R. C., Martini, E. M., and Petzhold, C. L. (2018). Reinforcing anticorrosive properties of biobased organic coatings through chemical functionalization with amino and aromatic groups. *Prog. Org. Coat.* 125, 372–383. doi: 10.1016/j.porgcoat.2018.09.021

Park, E. J., Yoon, H. S., Kim, D. H., Kim, Y. H., and Kim, Y. D. (2014). Preparation of self-cleaning surfaces with a dual functionality of superhydrophobicity and photocatalytic activity. *Appl. Surf. Sci.* 319, 367–371. doi: 10.1016/j.apsusc.2014.07.122

Polizos, G., Tuncer, E., Sauers, I., and More, K. L. (2011). Physical properties of epoxy resin/titanium dioxide nanocomposites. *Polym. Eng. Sci.* 51, 87–93. doi: 10.1002/pen.21783

Pouget, E., Tonnar, J., Lucas, P., Lacroix-Desmazes, P., Ganachaud, F., and Boutevin, B. (2009). Well-architectured poly (dimethylsiloxane)-containing copolymers obtained by radical chemistry. *Chem. Rev.* 110, 1233–1277. doi: 10.1021/cr8001998

Pourhashem, S., Vaezi, M. R., Rashidi, A., and Bagherzadeh, M. R. (2017). Exploring corrosion protection properties of solvent based epoxy-graphene oxide nanocomposite coatings on mild steel. *Corros. Sci.* 115, 78–92. doi: 10.1016/j.corsci.2016.11.008

Pugachevskii, M. (2013). Ultraviolet absorption spectrum of laser-ablated titanium dioxide nanoparticles. *Tech. Phys. Lett.* 39, 36–38. doi: 10.1134/S1063785013010239

Radoman, T. S., DŽunuzović, J. V., Jeremić, K. B., Grgur, B. N., Miličević, D. S., Popović, I. G., et al. (2014). Improvement of epoxy resin properties by incorporation of TiO2 nanoparticles surface modified with gallic acid esters. *Mater. Design* 62, 158–167. doi: 10.1016/j.matdes.2014.05.015

Radoman, T. S., Terzić, N., Spasojević, P. M., DŽunuzović, J. V., Marinković, A. D., Jeremić, K. B., et al. (2015). Synthesis and characterization of the surface modified titanium dioxide/epoxy nanocomposites. *Adv. Technol.* 4, 7–15. doi: 10.5937/savteh1501007R

Ramezanzadeh, B., Attar, M., and Farzam, M. (2011). A study on the anticorrosion performance of the epoxy–polyamide nanocomposites containing ZnO nanoparticles. *Prog. Org. Coat.* 72, 410–422. doi: 10.1016/j.porgcoat.2011.05.014

Ramezanzadeh, B., Haeri, Z., and Ramezanzadeh, M. (2016a). A facile route of making silica nanoparticles-covered graphene oxide nanohybrids (SiO2-GO); fabrication of SiO2-GO/epoxy composite coating with superior barrier and corrosion protection performance. *Chem. Eng. J.* 303, 511–528. doi: 10.1016/j.cej.2016.06.028

Ramezanzadeh, B., Niroumandrad, S., Ahmadi, A., Mahdavian, M., and Moghadam, M. M. (2016b). Enhancement of barrier and corrosion protection performance of an epoxy coating through wet transfer of amino functionalized graphene oxide. *Corros. Sci.* 103, 283–304. doi: 10.1016/j.corsci.2015.11.033

Rathod, P., and Waghuley, S. (2015). Synthesis and UV-Vis spectroscopic study of TiO2 nanoparticles. *Int. J. Nanomanuf.* 11, 185–193. doi: 10.1504/IJNM.2015.071925

Shen, S., and Zuo, Y. (2014). The improved performance of Mg-rich epoxy primer on AZ91D magnesium alloy by addition of ZnO. *Corros. Sci.* 87, 167–178. doi: 10.1016/j.corsci.2014.06.020

Shi, X., Nguyen, T. A., Suo, Z., Liu, Y., and Avci, R. (2009). Effect of nanoparticles on the anticorrosion and mechanical properties of epoxy coating. *Surf. Coat. Technol.* 204, 237–245. doi: 10.1016/j.surfcoat.2009.06.048

Sung, P.-H., and Lin, C.-Y. (1997). Polysiloxane modified epoxy polymer networks—I. Graft interpenetrating polymeric networks. *Eur. Polym. J.* 33, 903–906. doi: 10.1016/S0014-3057(96)00214-5

Vasei, M., Das, P., Cherfouth, H., Marsan, B., and Claverie, J. P. (2014). TiO2@ C core-shell nanoparticles formed by polymeric nano-encapsulation. *Front. Chem.* 2:47. doi: 10.3389/fchem.2014.00047

Vázquez-Velázquez, A., Velasco-Soto, M., Pérez-García, S., and Licea-Jiménez, L. (2018). Functionalization effect on polymer nanocomposite coatings based on TiO2-SiO2 nanoparticles with superhydrophilic properties. *Nanomaterials.* 8, 369. doi: 10.3390/nano8060369

Velan, T. T., and Bilal, I. M. (2000). Aliphatic amine cured PDMS-epoxy interpenetrating network system for high performance engineering applications—Development and characterization. *Bull. Mater. Sci.* 23, 425–429. doi: 10.1007/BF02708394

Verma, S., Mohanty, S., and Nayak, S. (2019). A review on protective polymeric coatings for marine applications. *J. Coat. Technol. Res.* 16, 307–338. doi: 10.1007/s11998-018-00174-2

Wang, C., Wang, H., Hu, Y., Liu, Z., Lv, C., Zhu, Y., et al. (2018). Anti-corrosive and scale inhibiting polymer-based functional coating with internal and external regulation of TiO2 Whiskers. *Coatings* 8:29. doi: 10.3390/coatings8010029

Yi, C., Rostron, P., Vahdati, N., Gunister, E., and Alfantazi, A. (2018). Curing kinetics and mechanical properties of epoxy based coatings: the influence of added solvent. *Prog. Org. Coat.* 124, 165–174. doi: 10.1016/j.porgcoat.2018.08.009

Zaarei, D., Sarabi, A. A., Sharif, F., and Kassiriha, S. M. (2008). Structure, properties and corrosion resistivity of polymeric nanocomposite coatings based on layered silicates. *J. Coat. Technol. Res.* 5, 241–249. doi: 10.1007/s11998-007-9065-5

Zhang, H., Bao, W., Deng, Z., Zhang, S., and Ji, Z. (2019). Next-generation composite coating system: nanocoating. *Front. Mater.* 6:72. doi: 10.3389/fmats.2019.00072

Zhang, X., Wang, F., and Du, Y. (2007). Effect of nano-sized titanium powder addition on corrosion performance of epoxy coatings. *Surf. Coat. Technol.* 201, 7241–7245. doi: 10.1016/j.surfcoat.2007.01.042

Zheng, S., Bellido-Aguilar, D. A., Huang, Y., Zeng, X., Zhang, Q., and Chen, Z. (2019). Mechanically robust hydrophobic bio-based epoxy coatings for anti-corrosion application. *Surf. Coat. Technol.* 363, 43–50. doi: 10.1016/j.surfcoat.2019.02.020

Zhu, G., Cui, X., Zhang, Y., Chen, S., Dong, M., Liu, H., et al. (2019). Poly (vinyl butyral)/graphene oxide/poly (methylhydrosiloxane) nanocomposite coating for improved aluminum alloy anticorrosion. *Polymer* 172, 415–422. doi: 10.1016/j.polymer.2019.03.056